Effects of Boundary Conditions on Magnetic Friction

Kentaro Sugimoto
Department of Physics, The University of Tokyo

January 9, 2018

I would like to thank Prof. Hatano for useful discussions. I am grateful to Dr. Hinokihara in the Miyashita group, Department of Physics, the University of Tokyo, for sharing his expertise on the parallel computing techniques. I also thank Dr. Tamura, National Institute for Material Science, for useful comments on precursors of critical phenomena in finite-size systems. I would also like to express my gratitude to the members of the Hatano group and my family for their moral support and warm encouragements.

Abstract

We numerically investigate magnetic friction in the non-equilibrium Ising model with the quasi-one-dimensional geometry. The upper half of the system slides against the lower half along the transverse axis with a fixed sliding velocity. We calculate the frictional force density and the bulk energy density. We find peaks in their temperature derivatives, which may diverge in the two-dimensional limit. The result is consistent with Ref. [1], which showed a novel boundary critical point above the ordinary bulk critical point in two dimensions.

Contents

Chapter 1

Introduction

In this chapter we introduce two of the most famous problems in analyzing the frictional force as problems of statistical mechanics, giving recent developments for solving them. We then pose another problem regarding *manipulation* of the sliding friction which occurs in highly lubricated solids. To this end we simplify our problem into a dimensional crossover in lattice systems.

The sliding friction in solids is a very complicated problem to analyze, despite the fact that our daily lives are linked with it in various forms. One reason of the difficulty is that there is no general theory which determines the most important microscopic degree of freedom to describe the macroscopic phenomenon of the sliding friction.

One may think that with the skill of statistical mechanics we can deal with the problem in a systematic manner. However, there are several essential problems including the following: (i) The sliding friction is essentially a non-equilibrium phenomenon (see Section 1.1); (ii) We cannot directly observe the sliding surface (see Section 1.2).

1.1 Sliding Frictions as Non-Equilibrium Problems

We can regard the sliding friction as the following elementary problem. We consider an object O and a substrate S, and let S slide against O by applying an external force $f_{\rm ext}$ to O. When O and S interact with each other, the kinetic energy of O given by the external force is expected to be lost through the interaction, and then the entire system of O and S heats up (if the system is closed) or the energy dissipates from the system to an external environment (if the system is open). In the latter case, when we control the external force $f_{\rm ext}$ to balance it with the frictional force $f_{\rm fric}$ the sliding velocity v becomes constant and the dissipation process becomes stationary. Then the frictional force $f_{\rm fric}$ can be considered as a function of the sliding velocity.

The standard method of statistical mechanics called the linear-response theory appears to solve the problem if the velocity is much smaller than the rate ξ/τ, where ξ and τ are the characteristic length and time of the system, respectively. However, we already know well that the static frictional force is non-zero for several systems, for which the frictional force

has a non-linear velocity dependence. This shows us that the complexity of the problem is beyond the linear-response theory.

Several model calculations and experiments have solved these problems, directly [1–18] and indirectly [19–22]. Phononic contributions to sliding frictions were analyzed with the Frenkel-Kontorova model [2, 3, 19–22] and simulated with cold atoms [4–6], whereas eletronic contributions were discovered [23] and explained within an image potential theory [7]. As a quantum phenomena, sliding friction between adsorbed helium atoms and its substrates [8–10] is recently getting attention, but their theoretical description is still not satisfactory and remains to be an open problem.

1.2 Impossibility of the Observation of the Sliding Surface

The dimensionality of the sliding surface is up to two, if that of the whole system is three. Sliding surfaces are different in many ways from the standard two-dimensional surfaces on three-dimensional solids which have been investigated for many years. In particular we cannot perform a direct observation of the sliding surface by apparatuses such as the standard microscope. The difficulty has prevented us from clarifying non-equilibrium properties of the sliding friction.

The frictional-force microscope have played important roles in investigating such sliding surfaces. This apparatus sees the roughness of the substrate by observing frictional force on its tips, by which we can recover the macroscopic frictional force as its integration over the surface. By the use of frictional-force microscopes, a local lateral force was measured by Ternes *et al.* [11] and *superlubricity* was observed by Urbakh [12] as an intriguing phenomenon in which the frictional force is strongly dependent on the sliding direction and almost vanishes in several directions.

1.3 Manipulating the Friction

As mentioned above, recent researches well revealed the nature of sliding frictions. This gave rise to new problems about the friction in atomically microscopic systems.

Ordinary frictions in solids are mostly governed by excitations of phonon degrees of freedom, because the sliding surface is almost always rougher than the scale of the atom. Once we lubricate the sliding surface highly, other degrees of freedom such as the orbital and the spin angular momenta of electrons emerge as additional contributions to the friction.

We are already familiar with the most remarkable example of such a system in our daily lives, namely *micro-electric mechanical systems* (**MEMS**). MEMS plays important roles in the printing head of inkjet printers, the accelerometer in smartphones and so on. MEMS has clean planes sliding with an accuracy of a micrometer or a nanometer [13–15], because of which they experience the friction with many kinds of degrees of freedom including not only phonon excitations but also other contributions such as electronic excitaions and electron-

phonon couplings. The small size of these systems results in a large friction, which lessens the working efficiency or disables the operation of MEMS, because the ratio of the surface area over the volume of the system becomes larger with the smaller size under a fixed geometry. In order to tackle with the issue of manipulation of the friction in small systems, we need to obtain more fundamental knowledge of the friction.

1.4 Magnetic Friction

The way to manipulate the friction in small systems is less understood than its nature. We here consider manipulating friction of magnetic materials by numerically simulating lattice models.

The nature of magnetic frictions was first revealed by Kadau *et al.* [16] by the use of the Ising model. Just after it, Fusco *et al.* [24] investigated magnetic frictions in the Heisenberg spin systems and a moving dipole moment on them. A crossover of the velocity dependence of the magnetic frictional force was revealed by Magiera *et al.* [17]. A direct observation of the magnetic frictions by a scanning probe microscopy was then performed by Wolter *et al.* [18].

In the present work we consider two strips of the quasi-one-dimensional Ising model sliding against each other with a fixed velocity. We discuss the difference of the frictional forces under two boundary conditions, namely the anti-parallel and the parallel, and its dependence on the distance between the two boundaries. We find a method of manipulating the friction using the different boundary conditions. These boundary conditions can be realized in experiments by aligning the boundary spins of sliding magnets.

Frictions in such models were considered first in a numerical study by Kadau *et al.* [16]. They revealed by Monte Carlo simulations that two square lattices of the Ising model which slide against each other experience the friction, depending on the temperature and the sliding velocity. Immediately after the research, it was revealed [1] that the Ising model goes under a non-trivial non-equilibrium phase transition (**NEPT**) in the high-velocity limit, where the two square lattices are decoupled in terms of the correlation between the two lattices and feel an effective mean field depending on the magnetization of each other [1]. This analysis showed that a novel critical point exists at a generally higher temperature than the ordinal critical point for models in arbitrary dimensions and geometries (see Chapter 2). They also developed a new dynamics [1] which enables an analytical treatment for finite sliding velocities, obtaining a non-equilibrium critical line.

Based on the results in Ref. [1], we consider a dimensional crossover from one dimension to two in Ising models with the two boundary conditions. In the one-dimensional limit the boundary conditions seem to have the maximum effect on the friction, whereas in the two-dimensional limit there seems to be no effects. The behaviors in the both limits for the free boundary conditions correspond to the results in Ref. [1].

Chapter 2

Velocity-driven Non-equilibrium Phase Transition in Ising Models

To discuss the non-equilibrium crossover between two different dimensionalities, we make a brief review of the exact results by Hucht [1]. His analysis is based on the fact that two Ising cylinders with relative motion make a novel mean-field, which leads the system to a non-trivial phase transition.

Let us consider two equivalent square lattices of the Ising model each of which contacts the other by one of its one-dimensional boundaries (see Fig. 2.1). We make one lattice slide along the contact plane against the other lattice with a constant velocity v. The entire system thereby goes into a non-equilibrium stationary state instead of equilibration. The non-equilibrium stationary state well describes the behavior of two magnetic materials with a friction. This setup is explained in detail in Chapter 3.

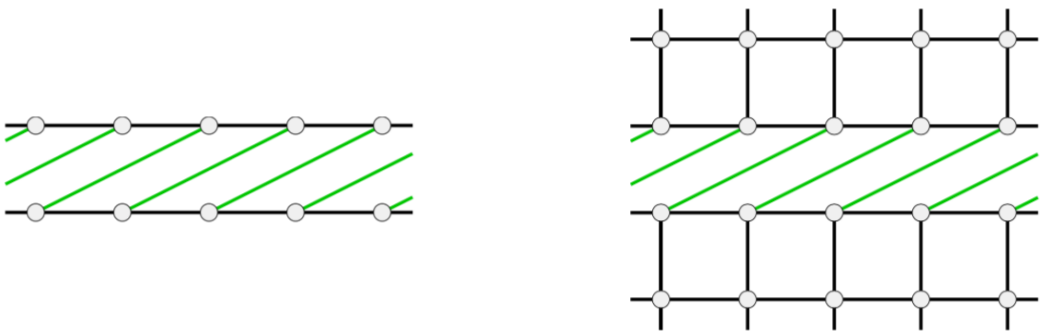

(a) (b)

Figure 2.1: Sketches of the models considered in Ref. [1][1]. Both cases depict a schematic view after the sliding by twice a lattice constant: (a) Two chains of the one-dimensional model; (b) Two square lattices of the two-dimensional model.

[1]Reprinted Figs. 2 and 3 with permission adapted from A. Hucht, Phys. Rev. E **80**, 061138 (2009). Copyright (2018) by the American Physical Society.

As a well known fact, the ordinary two-dimensional Ising model has an equilibrium phase transition at the critical temperature $T_{\mathrm{c,eq}} = 2/\left[\log\left(1+\sqrt{2}\right)\right] = 2.2691853\ldots$ in the thermodynamical limit. The system with the friction becomes equivalent to the equilibrium case in the limit of $v \to 0$. In addition to the ordinary phase transition, it was revealed [1, 16] that there exists a novel phase transition in which the magnetization grows on the sliding boundary (see Fig. 2.2). Now we denote the velocity-dependent non-equilibrium critical point by $T_{\mathrm{c}}(v)$ apart from the equilibrium critical point $T_{\mathrm{eq,c}}$. Hucht [1] claims that the critical temperature $T_{\mathrm{c}}(v)$ *deviates* from $T_{\mathrm{c,eq}}$ at the point $v = 0$ towards the limit $v = \infty$.

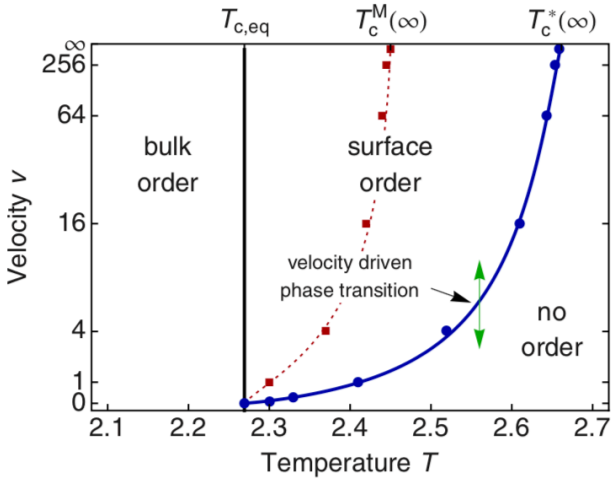

Figure 2.2: The phase diagram of the two-dimensional non-equilibrium Ising model obtained in Ref. [1][2]. The black solid line, the red dashed line and the blue solid line indicate the ordinary bulk phase transition $T_{\mathrm{c,eq}}$, a non-equilibrium boundary phase transition for the Metropolis rate $T_{\mathrm{c}}^{\mathrm{M}}(v)$ and one for the multiplicative rate $T_{\mathrm{c}}^{*}(v)$, respectively. From right to left across the non-equilibrium phase boundary the system acquires non-zero expectation value of magnetization on the sliding boundary.

This phenomenon wes first reported in the numerical results by Kadau *et al.* [16] using Monte Carlo simulations both on the Metropolis and the Glauber algorithms in a two-dimensional model, and then was investigated in a more analytic manner by Hucht [1] in several dimensionalities and model geometries. One of the important points of the latter result is that a mean-field analysis becomes exact for the *second* critical temperature in the limit $v \to \infty$ when we use a novel algorithm called the *multipricative rate*; this critical temperature is indicated as $T_{\mathrm{c}}^{*}(\infty)$ in Fig. 2.2. The use of the multipricative rate also enabled us to give an exact equation for $T_{\mathrm{c}}^{*}(v)$, which depends on the flip rate and the sliding velocity $v > 0$. Hucht additionally obtained the line $T_{\mathrm{c}}^{\mathrm{M}}(v)$ for the Metropolis rate numerically, which we will compare with our result in Chapter 4.

If the velocity v is much less than the rate $\xi_x^{(\mathrm{eq})}(\beta)/\tau_x^{(\mathrm{eq})}(\beta)$, we can expect the system to behave similarly to its equilibrium state, where $\xi_x^{(\mathrm{eq})}(\beta)$ and $\tau_x^{(\mathrm{eq})}(\beta)$ are the correlation

[2]Reprinted Fig. 15 with permission from A. Hucht, Phys. Rev. E **80**, 061138 (2009). Copyright (2018) by the American Physical Society.

length along the direction parallel to the sliding surface and the correlation time, respectively, for the equilibrium state at an inverse temperature $\beta := (k_{\rm B}T)^{-1}$. This corresponds to the case in which the pumped energy by the constant sliding quickly relaxes into the heat bath and the structure of domain walls near the sliding boundary is well sustained. On the other hand, the velocity v much greater than the rate $\xi_x^{(\rm eq)}(\beta)/\tau_x^{(\rm eq)}(\beta)$ should lead the system to a stationary state far from equilibrium, so that the structure near the sliding boundary is destroyed.

In the latter case a mean-field picture [1] well describes the behavior of the system; a set of the moving spins along the contact plane act on the other set of *relatively* moving spins as a spatially averaged effective field. It turns out that the self-consistent equation gives the exact critical temperature $T_{\rm c}^*(\infty)$ [1].

We summarize the result for one-dimensional chains and two-dimensional planes in order to discuss the crossover from one dimension to two dimensions in our models in Chapter 4. We first give a general Hamiltonian of the Ising model as follows:

$$\beta\mathcal{H}_\mu := -K\sum_{i<j}\sigma_i\sigma_j - h^{\rm ext}\sum_i\sigma_i - K\sum_i\mu_i\sigma_i, \tag{2.1}$$

where K, $h^{\rm ext}$ and μ_i with $\mu_i = \pm 1$ denote the exchange interaction, an external field and a stochastic field on the ith spin, respectively. The geometry of the model is either Fig. 2.1 (a) or (b). We assume that μ_i obeys a probability distribution $p_i(\mu_i)$ such that $\langle\mu_i\rangle := \sum_{\mu_i=\pm1} p_i(\mu_i)\mu_i = m_{\rm b}$ for a given value of $m_{\rm b}$. The form $p_i(\mu_i) := (1+\mu_i m_b)/2$ indeed satisfies the condition. If we decompose the Hamiltonian into the contribution of the stochastic field and the rest as

$$\beta\mathcal{H}_\mu = \beta\mathcal{H}_0 - K\sum_i\mu_i\sigma_i, \tag{2.2}$$

where

$$\beta\mathcal{H}_0 := -K\sum_{i<j}\sigma_i\sigma_j - h^{\rm ext}\sum_i\sigma_i, \tag{2.3}$$

the partition function of the system is written in the form

$$\mathcal{Z} = \left\langle {\rm Tr}_\sigma\left[{\rm e}^{-\beta\mathcal{H}_\mu}\right]\right\rangle = {\rm Tr}_\sigma\left[{\rm e}^{-\beta\mathcal{H}_0}\left\langle\prod_i {\rm e}^{K\mu_i\sigma_i}\right\rangle\right] \tag{2.4}$$

$$= \prod_j \cosh k_j\ {\rm Tr}_\sigma\left[{\rm e}^{-\beta\mathcal{H}_0}\prod_j(1+\sigma_i m_{\rm b}\tanh K)\right]. \tag{2.5}$$

Let us assume that the boundary magnetization of one sliding surface acts as an effective field $h_{\rm b}$ on the boundary magnetization of the other. The model then reduces to

$$\beta\mathcal{H}_{\rm eq} := -K\sum_{i<j}\sigma_i\sigma_j - h_{\rm b}\sum_i\sigma_i = \beta\mathcal{H}_0 - b\sum_i\sigma_i, \tag{2.6}$$

with $b := h_{\rm b} - h^{\rm ext}$, which relaxes toward the equilibrium state. Its partition function is written as

$$\mathcal{Z}_{\rm eq} = {\rm Tr}_\sigma \left[{\rm e}^{-\beta \mathcal{H}_{\rm eq}} \right] = {\rm Tr}_\sigma \left[{\rm e}^{\beta \mathcal{H}_0} \sum_i {\rm e}^{b\sigma_i} \right] \tag{2.7}$$

$$= \prod_i \cosh b \; {\rm Tr}_\sigma \left[{\rm e}^{-\beta \mathcal{H}_0} \prod_i (1 + \sigma_i \tanh b) \right]. \tag{2.8}$$

Comparing the right-hand sides of Eqs. (2.5) and (2.8), we have $\mathcal{Z} \propto \mathcal{Z}_{\rm eq}$ if it holds that $\tanh b = m_{\rm b} \tanh K$. We thus have

$$h_{\rm b} = \tanh^{-1} \left(m_{\rm b} \tanh K \right) \tag{2.9}$$

in the limit $h^{\rm ext} \to 0$. The boundary magnetization under a static field $h_{\rm b}$ has a form of

$$m_{\rm b,eq}(K, h_{\rm b}) := \frac{\partial}{\partial h_{\rm b}} \log \mathcal{Z}_{\rm eq}, \tag{2.10}$$

and thus we have

$$m_{\rm b,eq} \left(K, \tanh^{-1} \left(m_b \tanh K \right) \right) = m_b \tag{2.11}$$

as a self-consistent relation for m_b.

The critical point is given by

$$1 = \left. \frac{\partial m_{\rm b,eq}}{\partial m_{\rm b}} \right|_{m_{\rm b}=0}. \tag{2.12}$$

Expanding the left-hand side of Eq. (2.11) to the first order of $m_{\rm b}$ and using the condition (2.12), we have

$$m_{\rm b,eq} \left(K, 0 \right) + m_b \tanh \left(K \right) \left. \frac{\partial m_{\rm b,eq}}{\partial h_{\rm b}} \right|_{h_{\rm b}=0} = m_b. \tag{2.13}$$

With the definition of the equilibrium boundary susceptibility

$$\chi_{\rm b,eq}(K) := \partial m_{\rm b,eq} / \partial h_{\rm b} |_{h_{\rm b}=0} \tag{2.14}$$

and the fact $m_{\rm b,eq} \left(K, 0 \right) = 0$, we finally have

$$\tanh \left(K \right) \chi_{\rm b,eq}(K) = 1. \tag{2.15}$$

The condition (2.15) determines the non-equilibrium critical temperature $K = K_{\rm c}$. Using the exact expressions of the magnetization for the one-dimensional Ising model and the

boudnary magnetization for the two-dimensional model, we have the numerical solutions of the condition (2.15) as

$$K_{\mathrm{c}}{}^{-1} = \begin{cases} 2.2691853\ldots & \text{in one dimension,} \\ 2.6614725\ldots & \text{in two dimensions.} \end{cases} \tag{2.16}$$

The latter corresponds to $T_{\mathrm{c}}(\infty)$ in Fig. 2.2. The former, on the other hand, is the same value as in the two-dimensional *equilibrium* Ising model. The equilibrium boundary susceptibility of the one-dimensional Ising model is given by

$$\chi_{\mathrm{b,eq}}(K) = \mathrm{e}^{2K}, \tag{2.17}$$

which reduces Eq. (2.15) to the relation

$$\tanh(K)\,\mathrm{e}^{2K} = 1, \tag{2.18}$$

which gives the two-dimensional equilibrium critical point, accidentally as far as we understand. The non-equilibrium critical temperature in the two-dimensional model is higher than that in the one-dimensional one, because in general the effect of the mean-field is stronger for higher dimensions under the same perturbation.

Note that the temperature K_{c} corresponds to the non-equilibrium critical temperature in the limit $v \to \infty$, and is consistent with the extrapolation from the results for two dimensions with the multipricative rate (see Fig. 2.2).

Chapter 3

Numerical Simulations

3.1 Setup of the Model

Sliding friction is a form of energy dissipation on the surface between a moving object and its substrate. The dissipated energy is originated in the kinetic energy of the moving object. We here consider a constantly moving case in which an external force maintains the motion of the object with endless supply of its kinetic energy. This view leads to its *non-equilibrium stationary state*. When the system is in a non-equilibrium stationary state, it is often easy to calculate *energy currents* such as the frictional heat, its power and so on. Applying the view to our case in which two square lattices of the Ising model slide against each other, we can formulate the problem as follows; see Fig. 3.1.

1. We prepare a square lattice of the Ising model of size $L_x \times L_z$ and impose periodic boundary conditions in the transverse (x) direction, whereas we set the open boundary conditions in the longitudinal (z) direction for the moment. We first set the system in the equilibrium state of a temperature T.

2. We cut the system along the x-direction into two parts, maintaining interactions on the cut.

3. We slide two parts along the cut plane with relative velocity v. In other words, we shift the upper half by a lattice constant every $1/v$ unit time.

The Hamiltonian of the system is given by

$$H = H_{\text{upper}} + H_{\text{lower}} + H_{\text{slip}}(t), \tag{3.1}$$

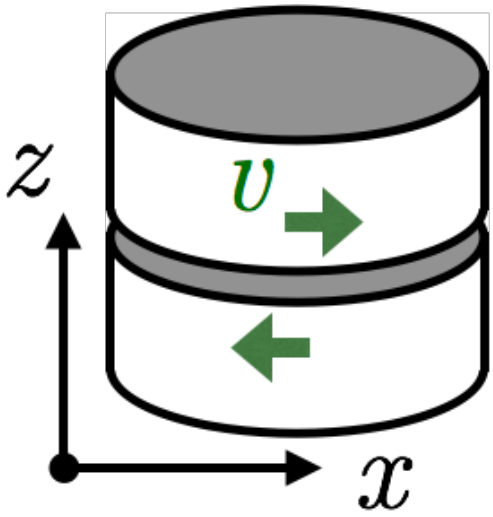

Figure 3.1: Two cylinders of the Ising model sliding with the velocity v.

where

$$H_{\text{upper}} := -J \sum_{\langle i,j\rangle \in \text{upper}} \sigma_i \sigma_j, \tag{3.2}$$

$$H_{\text{lower}} := -J \sum_{\langle i,j\rangle \in \text{lower}} \sigma_i \sigma_j, \tag{3.3}$$

$$H_{\text{slip}}(t) := -J \sum_{\langle i,j(t)\rangle \in \text{slip}} \sigma_i \sigma_{j(t)} \tag{3.4}$$

with the subscripts upper, lower and slip representing the set of neighboring spin pairs on the upper half, the lower half and the slip plane, respectively.

Shift operations lead the system to repeated *pumping* and *dissipation* processes as follows:

1. **Shift**: A shift operation excites the energy on the slip plane by the amount $\langle H_{\text{slip}}(t') - H_{\text{slip}}(t)\rangle_{\text{st}}$. The letter t' denotes the time just after the shift operation at time t.

2. **Relax 1**: The excited energy on the slip plane $\langle H_{\text{slip}}(t') - H_{\text{slip}}(t)\rangle_{\text{st}}$ dissipates to the entire system.

3. **Relax 2**: The excited entire system relaxes towards the equilibrium.

Our model always reaches a non-equilibrium stationary states in the long-time limit $t \to \infty$, which depends on the temperature T and the sliding velocity v; see Sec. 3.3.2 for the proof. We define the stationary state average $\langle A\rangle_{\text{st}} := \sum_i A_i p_i^{(\text{st})}$ for an arbitrary observable A, where $\{A_i\}$ are observed values of A and $p_i^{(\text{st})}$ denotes the stationary-state probability distribution, which is different from the equilibrium (canonical) probability distribution $p_i^{(\text{eq})} \propto \exp\left[-E_i/k_{\text{B}}T\right]$.

3.2 Definitions of Physical Quantities

The excited and relaxed amounts of energy per unit time correspond to the energy pumping and dissipation, respectively. The energy pumping $P(t)$ and the energy dissipation $D(t)$ are given by

$$P(t) := \sum_{i_v=0}^{v-1} \left[H_{\rm slip}\left(t' - 1 + \frac{i_v}{v}\right) - H_{\rm slip}\left(t - 1 + \frac{i_v}{v}\right) \right], \tag{3.5}$$

$$D(t) := \sum_{i_v=0}^{v-1} \left[H\left(t - 1 + \frac{i_v + 1}{v}\right) - H\left(t' - 1 + \frac{i_v}{v}\right) \right], \tag{3.6}$$

respectively. They correspond to the energy differences due to the **Shift** and the **Relax** processes. Note that we obtain the former and the latter by the slip plane and the entire system, respectively, and that the absolute values of $P(t)$ and $D(t)$ become equal to each other in the non-equilibrium stationary state.

We now consider the case in which the system is in a non-equilibrium stationary state. We denote by $P(L_x, L_z, T)$ and $D(L_x, L_z, T)$ the long-time limit of the energy pumping $P(t)$ and the energy dissipation $D(t)$, respectively, for a system of size $L_x \times L_z$ at the temperature T: $P(L_x, L_z, T) = \langle P(t) \rangle_{\rm st}$, $D(L_x, L_z, T) = \langle D(t) \rangle_{\rm st}$. We define the frictional force density $f(L_z, T)$ by

$$f(L_z, T) := \lim_{L_x \to \infty} \frac{F(L_x, L_z, T)}{L_x}, \tag{3.7}$$

where $F(L_x, L_z, T)$ is the long-time limit of the frictional force. We can calculate the frictional force $F(L_x, L_z, T)$ using its power $D(L_x, L_z, T)$ by the formula

$$F(L_x, L_z, T) = \frac{D(L_x, L_z, T)}{v}. \tag{3.8}$$

We can verify the formula (3.8) by considering general cases in which the frictional force and its power are both time dependent. Denoting the frictional force $F(x)$ at the position x, we have

$$\int_{t_0}^{t_1} dt\ D(t) = \int_{x(t_0)}^{x(t_1)} dx\ F(x) = \int_{t_0}^{t_1} \frac{dx}{dt} dt\ F(x(t)) = v \int_{t_0}^{t_1} dt\ F(x(t)) \tag{3.9}$$

for a time-dependent $D(t)$, because $dx/dt = v$. Under the assumption of a non-equilibrium stationary state, the integrands in both-hand sides of the relation (3.9) are still equal to each other in the long-time limit, and hence we have

$$D(L_x, L_z, T) = vF(L_x, L_z, T). \tag{3.10}$$

We use the fact that $\lim_{t\to\infty} |D(t)| = \lim_{t\to\infty} |P(t)|$ in order to estimate $D(t)$ because the Monte Carlo estimate of $P(t)$ has less statistical fluctuation [17, 25, 26]. In the long-time

limit, we therefore have

$$f(L_x, L_z, T) = \lim_{L_x \to \infty} \frac{P(L_x, L_z, T)}{v L_x}. \tag{3.11}$$

We also define the bulk energy density $\epsilon_{\mathrm{b}}(L_z, T)$ as follows:

$$\epsilon_{\mathrm{b}}(L_z, T) := \lim_{L_x \to \infty} \frac{E_{\mathrm{b}}(L_x, L_z, T)}{L_x L_z}, \tag{3.12}$$

where $E_{\mathrm{b}}(L_x, L_z, T)$ is the energy of the entire system. From this, we define the bulk heat capacity $c_{\mathrm{b}}(L_z, T)$ as follows:

$$c_{\mathrm{b}}(L_z, T) := \frac{\partial \epsilon_{\mathrm{b}}(L_z, T)}{\partial T}. \tag{3.13}$$

3.3 Non-equilibrium Monte Carlo Simulation

The dissipation process towards the heat bath occurs via a spin flip. This fundamental processes do not only describe the equilibrium state but also the non-equilibrium stationary state at a fixed temperature T [27]. Using the Monte Carlo method, we simulate this process.

3.3.1 Introduction of the Time Scale to Ising Models

In order to calculate dynamical observables such as the frictional power (3.5) and its dissipation rate (3.6), we have to define *a unit time* for the simulation of the finite-size system.

For the equilibrium Monte Carlo simulation, the most naive approach for the equilibrium state is the single-spin-flip algorithm, where we perform the sequence of a random selection of a spin and its flip with a temperature-dependent probability $p(T)$. We use the probability that satisfies the *detailed balanced condition*, which certainly leads the system towards the true equilibrium state with enough repetition of the sequence. For example, we often use the Metropolis probability $p_{\mathrm{M}}(T) := \min\{1, \mathrm{e}^{-\frac{\Delta E}{k_{\mathrm{B}} T}}\}$ as the probability $p(T)$, where ΔE is the energy difference due to the flip. We often call a *Monte Carlo step* a single process of the algorithm, and define a *Monte Carlo sweep* by N Monte Carlo steps, where N is the number of spins.

Which should we use as a unit time, a Monte Carlo step or a Monte Carlo sweep? Its answer can be found in the following manner. We usually assume that a statistical mechanical system is coupled to a heat bath by every local degree of freedom. The temperature of the system is kept constant by the heat bath, and the system exchanges its energy with the heat bath through local degrees of freedom. It is most natural to assume that the equilibrium relaxation of a macroscopic system takes place in the same time scale if the volume of the system is doubled. Thus the number of times of the energy exchanges is proportional to the total number of degrees of freedom of the system. This justifies to define a unit time by a Monte Carlo sweep; the relaxation time would be proportional to the total number of degrees of freedom if we used the Monte Carlo steps for a unit time.

3.3.2 Slip Plane with the Velocity v

Using the introduced time scale, we can also introduce the sliding velocity v of the system with N spins, where $N = L_x \times L_z$. Corresponding to the setup in Sec. 3.1, we perform an extended single-spin-flip algorithm as follows:

1. **Shift**: We shift the upper half of the lattice by a lattice constant.
2. **Flip**: We perform ordinary single flips for (N/v) times, which is the $(1/v)$ fraction of a Monte Carlo sweep.
3. We repeat the processes 1 and 2 for v times.

In the extended algorithm, the upper half slides with the velocity v in a unit time at regular intervals. The frictional power $P(t)$ and the dissipation rate $D(t)$ are measured in Monte Carlo simulations as the energy differences for a unit time due to the shift and the flip operation, respectively. Both observables have the same absolute value in the long-time limit.

We prove that this algorithm leads the system of any size to a non-equilibrium stationary state which depends on the temperature T and the velocity v. The above algorithm is represented by the following matrix for a Monte Carlo sweep:

$$\hat{T}(\beta, v) := \left[\left(\hat{M}(\beta) \right)^{N/v} \hat{S} \right]^{v}, \tag{3.14}$$

where $v \in \{\text{Divisors of } N\}$. The matrix $\hat{M}(\beta)$ and $\hat{S}$ express a Monte Carlo step at a temperature T and sliding of the upper half by a lattice constant, respectively, for the model of size $N = L_x \times L_z$. The matrix $\hat{T}(\beta, v)$ describes the time evolution for a Monte Carlo sweep, because the matrix have the Nth power of $\hat{M}(\beta)$. We now decompose the matrix $\hat{T}(\beta, v)$ into the $(1/v)$ fraction $\left(\hat{M}(\beta) \right)^{N/v} \hat{S}$. The matrices $\hat{M}(\beta)$ and $\hat{S}$ belong to the class called *stochastic matrices*, whose definition is given by following properties:

- Each element is greater than or equal to zero;
- Each row-wise total sum of elements is normalized to unity.

The product of two stochastic matrices is also a stochastic matrix. Indeed if we have two Ω-dimensional stochastic matrices $\hat{A}$ and $\hat{B}$, we have

$$\sum_{i=1}^{\Omega} (\hat{A}\hat{B})_{ij} = \sum_{i=1}^{\Omega} \sum_{k=1}^{\Omega} A_{ik} B_{kj} = \sum_{k=1}^{\Omega} \left(\sum_{i=1}^{\Omega} A_{ik} \right) B_{kj} = \sum_{k=1}^{\Omega} B_{kj} = 1 \quad \text{for } 1 \leq j \leq \Omega, \tag{3.15}$$

and therefore the matrix $\left(\hat{M}(\beta) \right)^{N/v} \hat{S}$ is also a stochastic matrix. Any stochastic matrix has at least the eigenvalue 1 (see App. A), and therefore the matrix $\left(\hat{M}(\beta) \right)^{N/v} \hat{S}$ has also

the eigenvalue 1. Our simulations therefore reach a unique non-equilibrium stationary state with the temperature T and the velocity v from *arbitrary* initial states.

The matrices $\hat{M}(\beta)$ and $\hat{S}$ have sparse structures as demonstrated in Figs. 3.2(a) and (b), respectively, whereas the matrix $\hat{T}(\beta, v)$ has a dense structure as in Fig. 3.2(c). The task of diagonalizing the matrix $\hat{T}(\beta, v)$ is the same as that of $\left(\hat{M}(\beta)\right)^{N/v} \hat{S}$, which corresponds to the time evolution for the $(1/v)$ fraction of a Monte Carlo sweep. We show in Fig. 3.3 the eigenvalue distributions of $\left(\hat{M}(\beta)\right)^{N/v}$ and $\left(\hat{M}(\beta)\right)^{N/v} \hat{S}$ for the model of size $L_x = 3, L_z = 2$. These eigenvalue distributions are somewhat similar to each other, reflecting that both of them correspond to the time evolution for the same time.

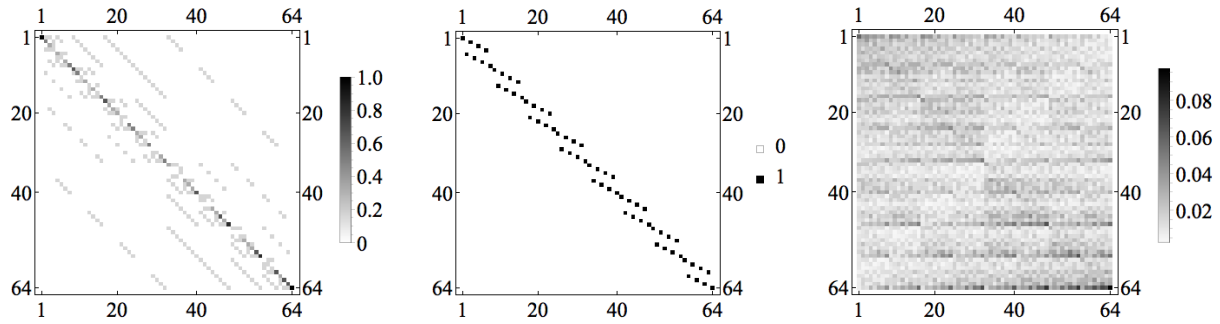

(a) (b) (c)

Figure 3.2: The array plots of matrices for the model of size $L_x = 3, L_z = 2$ and at the temperature $T = 10$: (a) $\hat{M}(\beta)$; (b) $\hat{S}$; (c) $\hat{T}(\beta, v)$.

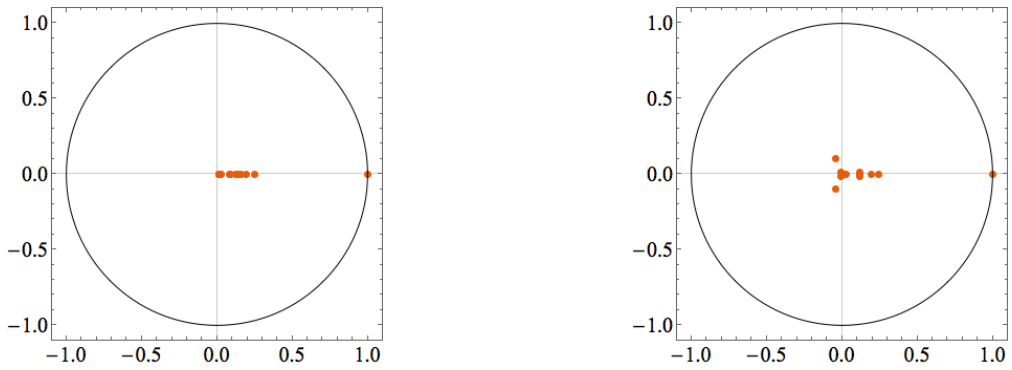

(a) (b)

Figure 3.3: Eigenvalue distributions of matrices for the model of size $L_x = 3, L_z = 2$ and at the temperature $T = 10$: (a) $\left\{\hat{M}(\beta)\right\}^{N/v}$; (b) $\left\{\hat{M}(\beta)\right\}^{N/v} \hat{S}$.

Chapter 4

Results

In this chapter, we first show the numerical results of the frictional force density $f(L_z, T)$, the bulk energy density $\epsilon_{\rm b}(L_z, T)$ and their temperature derivatives. We also show in Subsec. 4.2) the numerical infinite-size limit $L_x \to \infty$ converges with L_z and T fixed.

The range of parameters in our simulation is as follows. We computed the value of $f(L_z, T)$ for temperatures $k_{\rm B}T/J \in \{0.0, 0.1, 0.2, \ldots, 1.9, 2.0, 2.02, 2.04, \ldots, 2.48, 2.50, 2.6, 2.7, \ldots, 5.0\}$ and sizes $L_z \in \{4, 8, 16, 32, 64\}$ with the anti-parallel and the parallel boundary conditions. For the anti-parallel boundary conditions, we set the initial state to the domain-wall state, where spin variables σ_i in the upper half of the system are the same value as the spins on the upper boundary and those in the lower half as the spins on the lower boundary. For the parallel boundary conditions we set the initial state is set to the magnetized state, where all spin variables σ_i are the same value as both of boundaries. The reason why we used these initial states is that they are the most natural ground states which correpond to each boundary condition.

All the simulations are performed by the single-flip algorithm with the Metropolis rate. To obtain the observables in the non-equilibrium stationary state, we performed the equilibration process for 5000 sweeps and the stationarization process for 5000 sweeps for all given parameters. We checked the convergence of the observables to the equilibrium value and the stationary value for these time regions by fitting the observables by the function $A(t) = A_0 + A_1 {\rm e}^{-t/\tau}$. The duration of 5000 sweeps is substantially longer than the fitting parameter τ, which we call the *non-equilibrium relaxation time*. We performed these simulations for 480 samples for all parameters and averaged them, and then averaged along the time direction. The statistical errors of the data presented in the present chapter are all smaller than the point size.

4.1 Observed Quantities

4.1.1 Frictional Force Density $f(L_z, T)$

We show the behavior of the frictional force density $f(L_z, T)$ in Fig. 4.1. For both boundary conditions, $f(L_z, T)$ reaches the results in Ref. [16] with the size $L_z = 64$. We thereby decide

that the size $L_z = 64$ is a good approximation for the limit of $L_z \to \infty$. Towards this limit, $f(L_z, T)$ increases for the anti-parallel boundary conditions, whereas $f(L_z, T)$ decreases for the parallel boundary.

When the size L_z is larger than the correlation length $\xi_z(\beta)$ along the z direction, the system behaves as a two-dimensional one and the effects of the boundary conditions vanish, whereas when the size L_z is smaller than $\xi_z(\beta)$ the system is effectively one-dimensional. We can consider this behavior as a size-driven dimensional crossover.

4.1.2 Bulk Energy Density $\epsilon_{\rm b}(L_z, T)$

We show the behavior of the bulk energy density $\epsilon_{\rm b}(L_z, T)$ in Fig. 4.2. As the frictional force density $f(L_z, T)$, bulk energy densities $\epsilon_{\rm b}(L_z, T)$ also indicates asymptotic behavior in the limit of $L_z \to \infty$ and difference for small L_z, reflecting the dimensional crossover.

4.1.3 Temperature Derivatives $\partial f(L_z, T)/\partial T$ and $c_{\rm b}(L_z, T)$

We additionally show the behavior of temperature derivatives $\partial f(L_z, T)/\partial T$ and $c_{\rm b}(L_z, T) = \partial \epsilon_{\rm b}(L_z, T)/\partial T$ in Figs. 4.3 and 4.4, respectively.

The temperature derivative $\partial f(L_z, T)/\partial T$ and the temperature derivative $c_{\rm b}(L_z, T)$ exhibit sharp peaks at a characteristic temperature $T = 2.40$ (see the red marker line in Fig. 4.3) and $T = 2.27$ (see the black marker line in Fig. 4.4), respectively, for both boundary conditions for the largest size $L_z = 64$. This implies that they diverge in the limit of $L_z \to \infty$. We observe that the finite-size peak $T_{\rm peak}(L_z)$ shifts to lower temperatures for the anti-parallel boundary conditions and to higher temperatures for the parallel boundary conditions. This observation shows us that the anti-parallel boundary conditions acts as a *disordering* field such that the effective temperature of the system rises, while the parallel boundary conditions acts as an *ordering* field such that the effective temperature of the system drops. The changes in the effective temperature of the system are most enhanced for small L_z.

The peak locations $T = 2.40$ and $T = 2.27$ show good agreements with the non-equilibrium phase transition point $T_{\rm c}^{\rm M}(v)$ with the velocity $v = 10$ and the bulk phase transition point, respectively, in Ref. [1]; see Fig. 4.5. We can regard both divergent behaviors as intrinsic phase transitions independent of the boundary conditions, because the effect of boundary conditions vanishes in the limit of $L_z \to \infty$.

We also consider the reason why not only the heat capacity $c_{\rm b}(L_z, T)$ but also the temperature derivative of the frictional force density $\partial f(L_z, T)/\partial T$ shows the divergent behavior. The frictional force density $f(L_z, T)$ is estimated by the difference between the expectation value of the energy before and after the sliding. Then it is plausible that both expectation values have a singularity near $T = 2.40$, and these singularities do not cancel with each other.

[1] Reprinted Fig. 15 with permission adapted from A. Hucht, Phys. Rev. E **80**, 061138 (2009). Copyright (2018) by the American Physical Society.

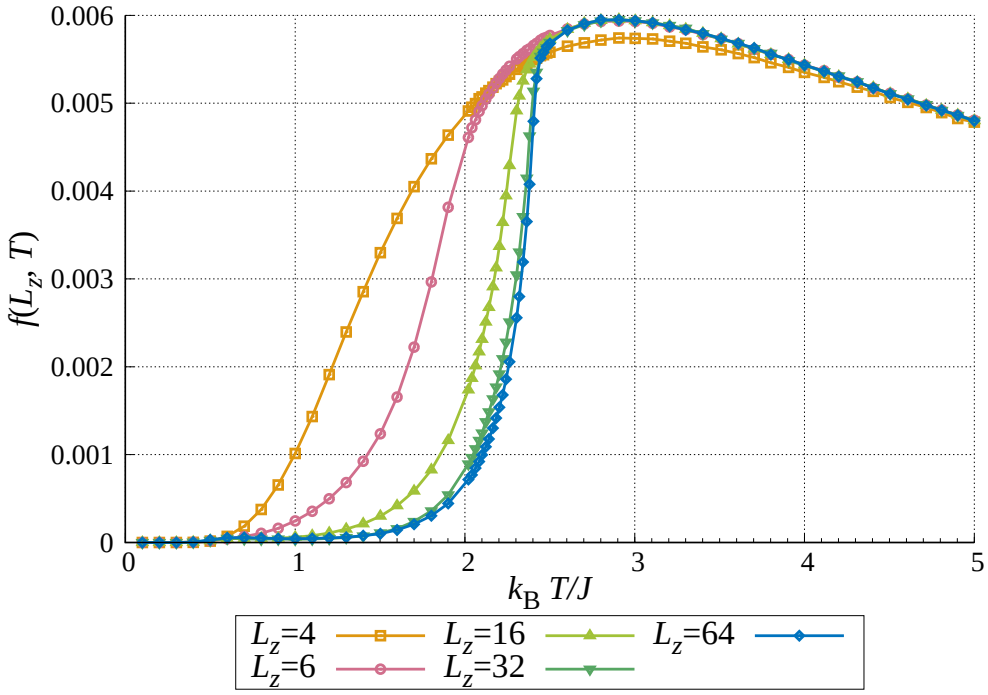

(a)

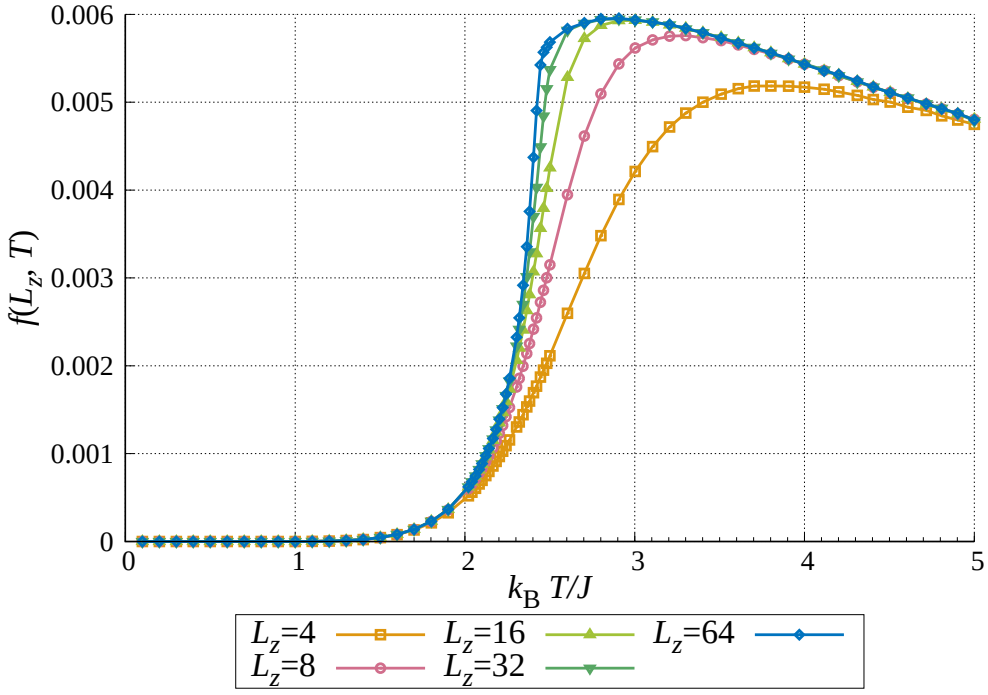

(b)

Figure 4.1: Temperature dependence of $f(L_z, T)$ with each boundary condition: (a) The anti-parallel boundary conditions; (b) The parallel boundary conditions.

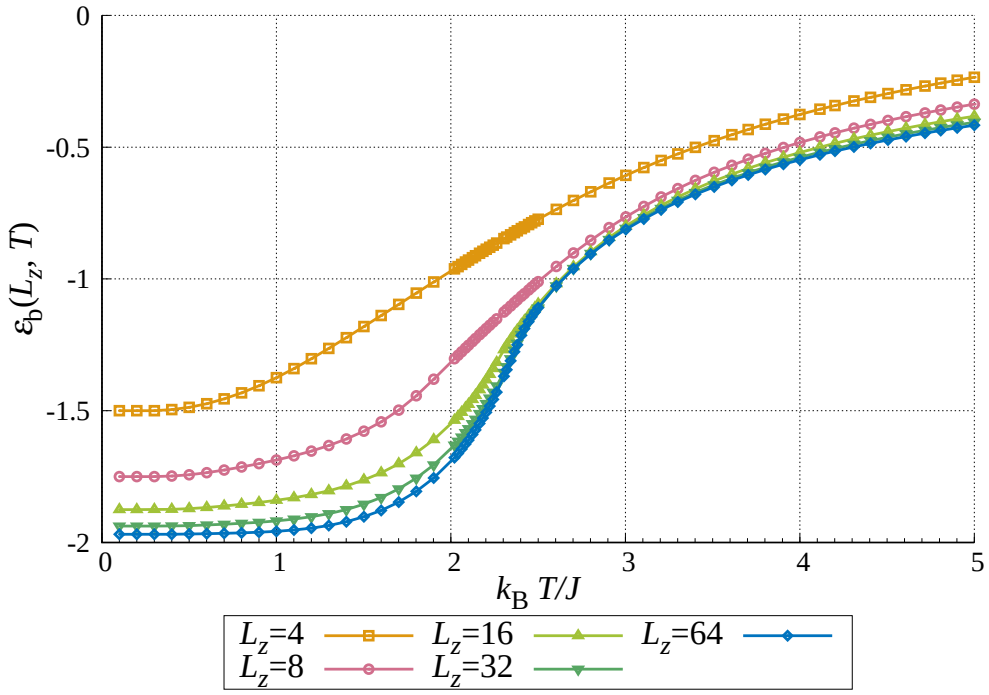

(a)

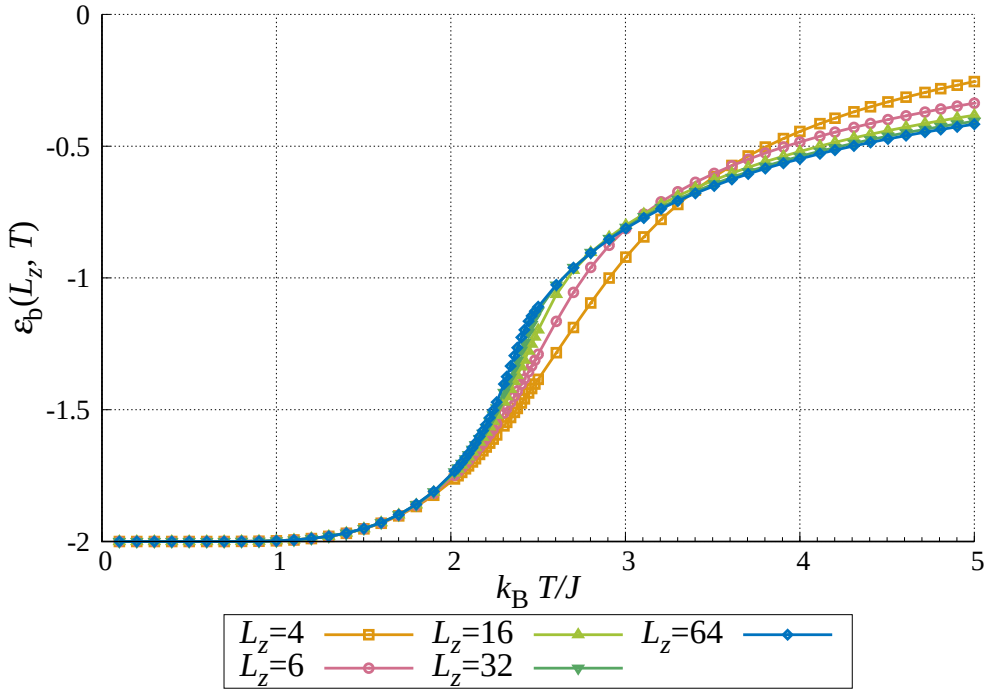

(b)

Figure 4.2: Temperature dependences of $\epsilon_b(L_z, T)$ with each boundary condition: (a) The anti-parallel boundary conditions; (b) The parallel boundary conditions.

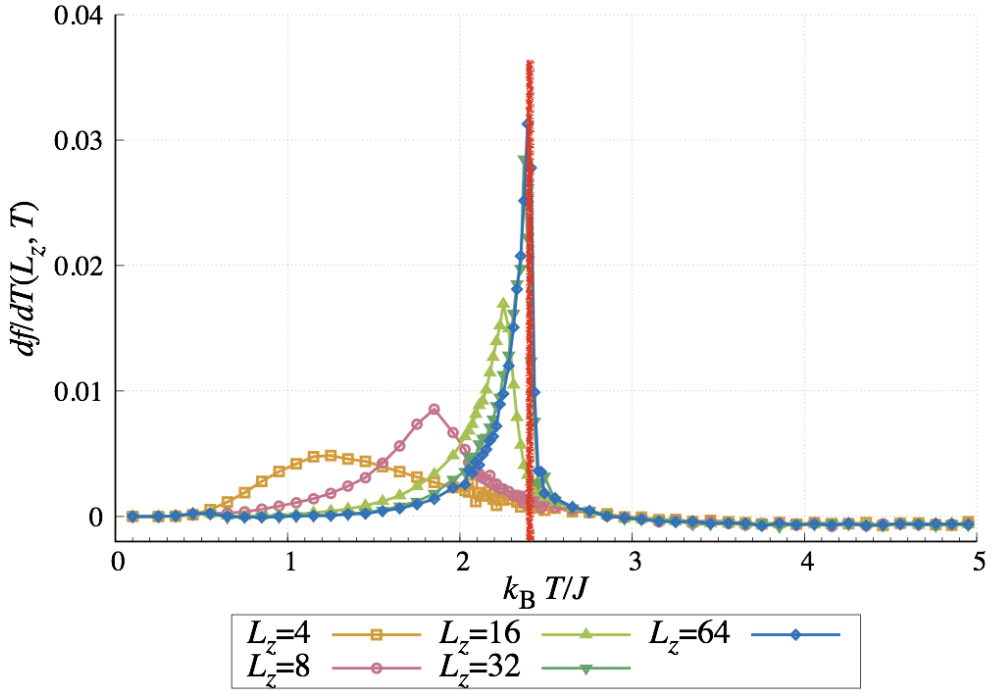

(a)

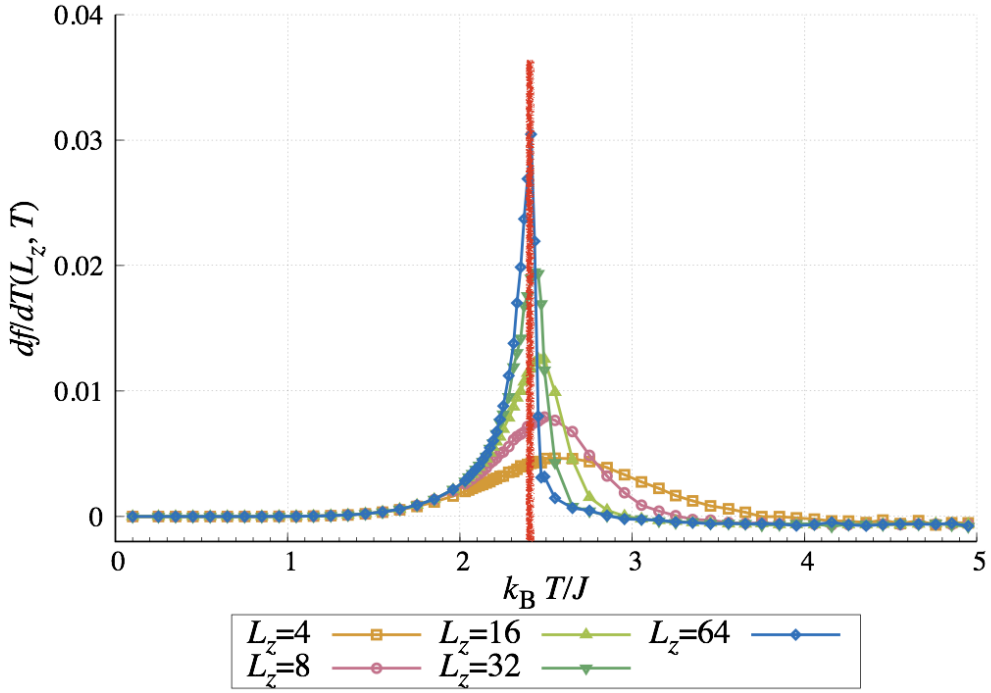

(b)

Figure 4.3: Temperature dependence of $\partial f(L_z, T)/\partial T$ with each boundary condition: (a) The anti-parallel boundary conditions; (b) The parallel boundary conditions. The vertical red line in each panel indicates the non-equilibrium critical temperature $T_c^{\mathrm{M}}(10) \simeq 2.40$ in the phase diagram of the two-dimensional non-equilibrium Ising model obtained in Ref. [1]; see Fig. 4.5.

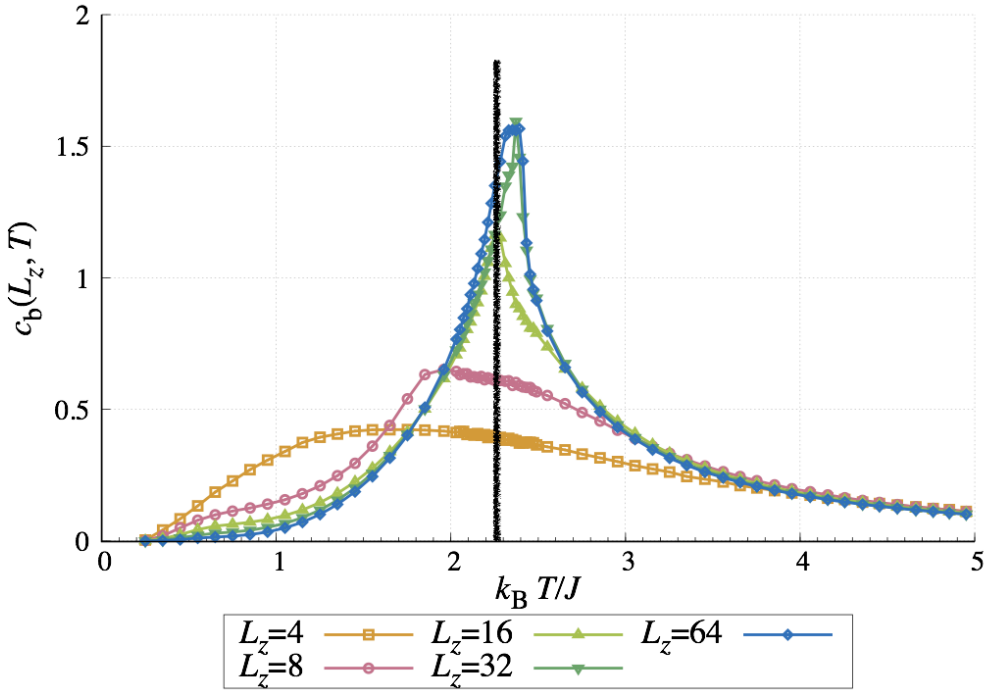

(a)

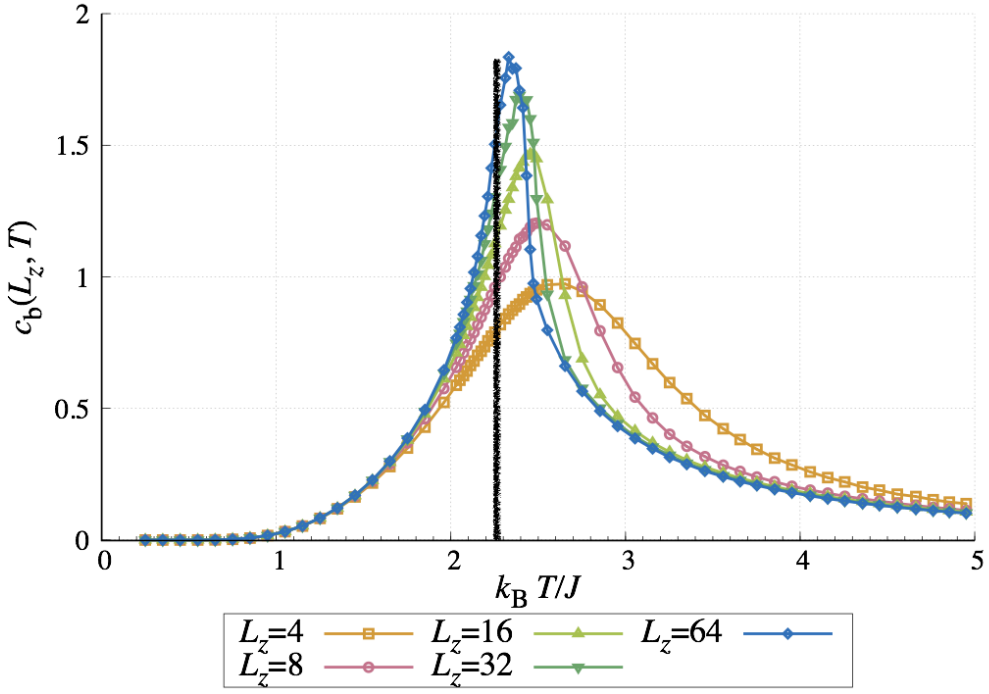

(b)

Figure 4.4: Temperature dependences of $c_{\rm b}(L_z, T) = \partial\epsilon_{\rm b}(L_z, T)/\partial T$ with each boundary condition: (a) The anti-parallel boundary conditions; (b) The parallel boundary conditions. The vertical black line in each panel indicates the equilibrium critical temperature $T_{\rm c,eq} \simeq 2.27$; see Fig. 4.5.

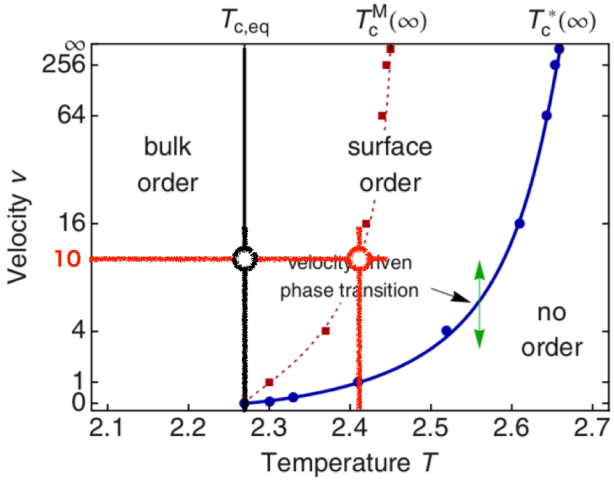

Figure 4.5: The non-equilibrium critical temperature $T_c^M(v) \simeq 2.40$ (the vertical red line) with the velocity $v \simeq 10$ and the equilibrium critical temperature $T_{c,eq} \simeq 2.27$ (the vertical black line) in the phase diagram of the two-dimensional non-equilibrium Ising model obtained in Ref. [1][1].

4.2 Checking the Convergence in the Limit $L_x \to \infty$

We now demonstrate that the following two observables converge in the infinite-size limit $L_x \to \infty$:

$$f(L_z, T) := \lim_{L_x \to \infty} \frac{F(L_x, L_z, T)}{L_x}, \tag{4.1}$$

$$\epsilon_b(L_z, T) := \lim_{L_x \to \infty} \frac{E_b(L_x.L_z, T)}{L_x L_z}. \tag{4.2}$$

We use the aspect ratios of $L_x = 30 \times L_z, 40 \times L_z, 50 \times L_z$ with L_z fixed in order to check the convergence in the limit $L_x/L_z \to \infty$. We show that the quantities $F(L_x, L_z, T)/L_x$ and $E_b(L_x, L_z, T)/L_x$ for each boundary conditions have little dependence on L_x for sufficiently large size of L_x with each size of L_z. Figures 4.6, 4.7, 4.8 and 4.9 respectively show the temperature dependence of the frictional force density and the energy density under each boundary condition for each size of $L_z = 4, 8, 16, 32, 64$.

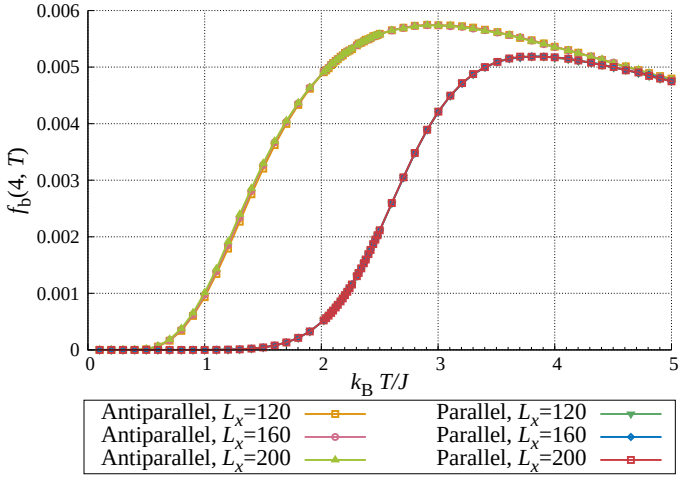

(a)

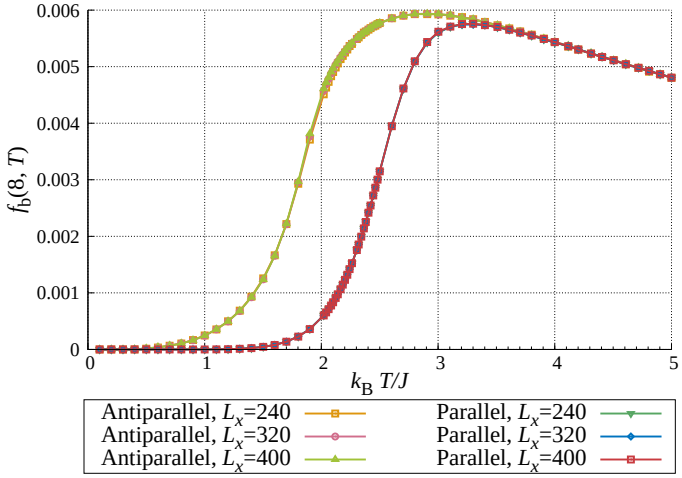

(b)

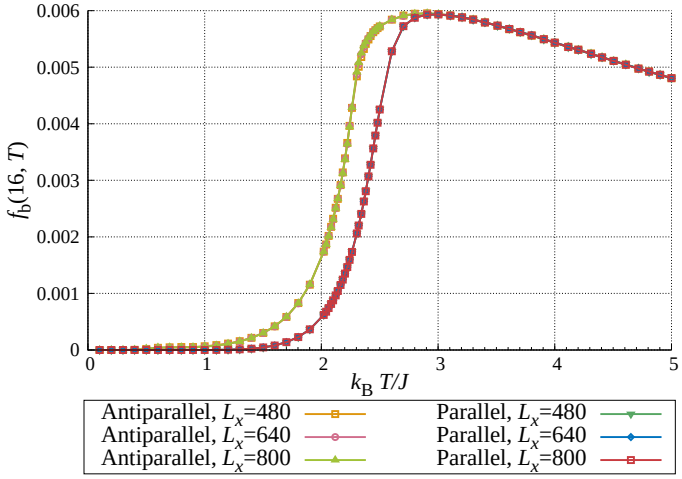

(c)

Figure 4.6: Each panel shows $F(L_x, L_z, T)/L_x$ against the temperature T: (a) $L_z = 4$; (b) $L_z = 8$; (c) $L_z = 16$.

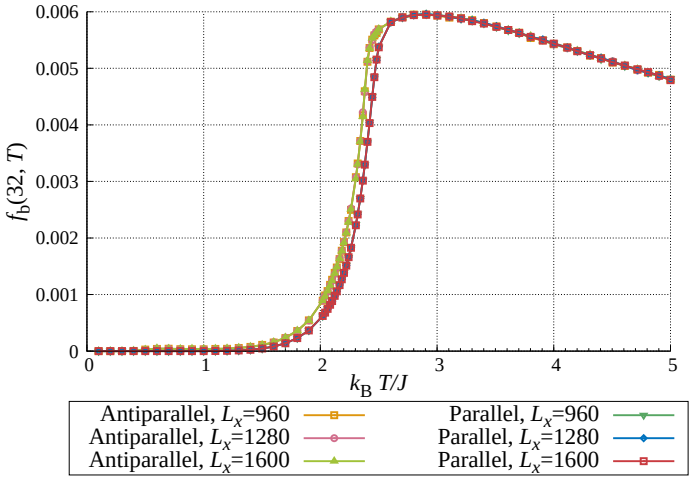

(a)

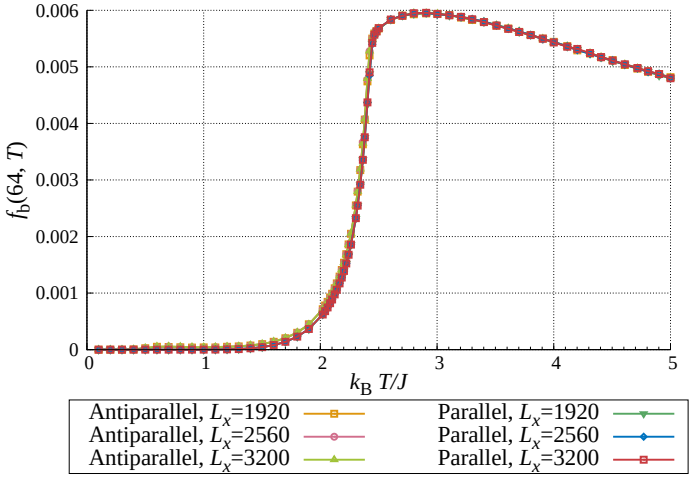

(b)

Figure 4.7: Each panel shows $F(L_x, L_z, T)/L_x$ against the temperature T: (a) $L_z = 32$; (b) $L_z = 64$.

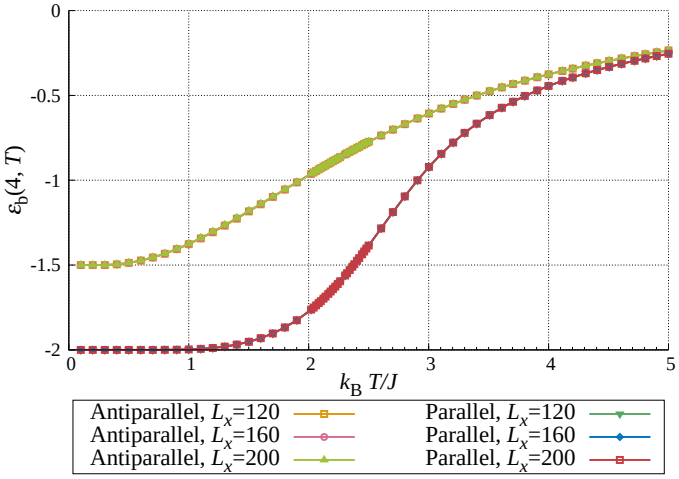

(a)

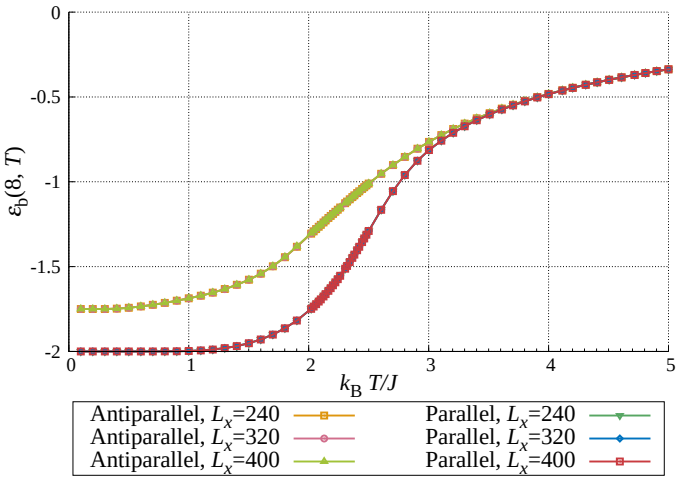

(b)

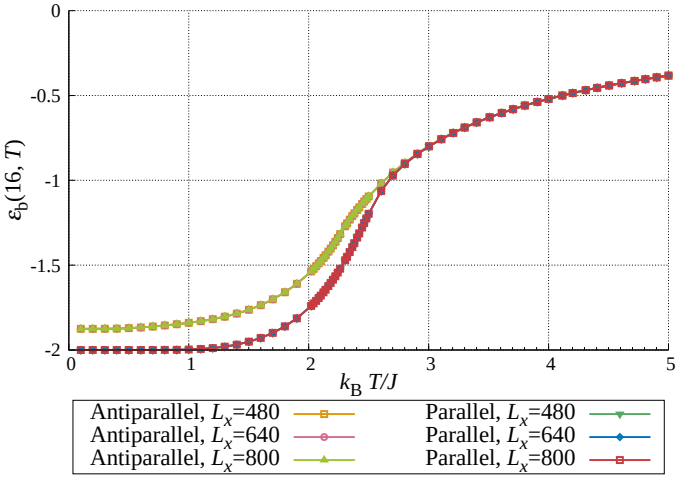

(c)

Figure 4.8: Each panel shows $E(L_x, L_z, T)/(L_x L_z)$ against the temperature T: (a) $L_z = 4$; (b) $L_z = 8$; (c) $L_z = 16$.

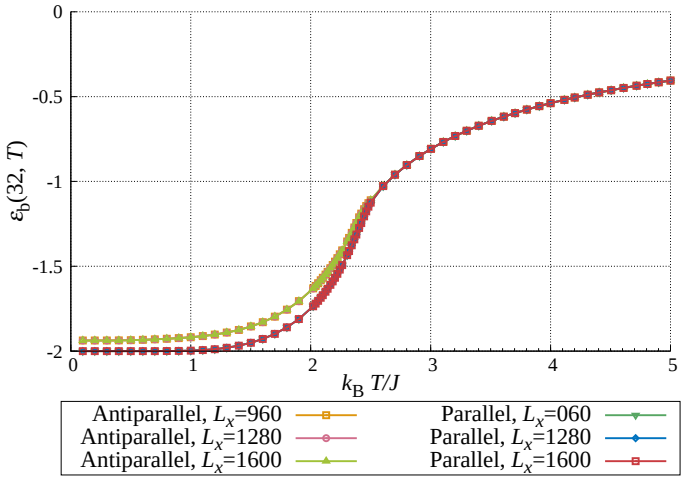

(a)

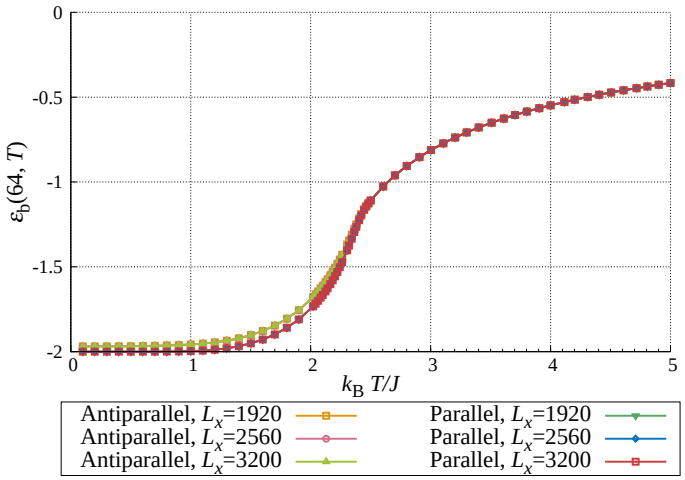

(b)

Figure 4.9: Each panel shows $E(L_x, L_z, T)/(L_x L_z)$ against the temperature T: (a) $L_z = 32$; (b) $L_z = 64$.

Chapter 5

Summary and Discussion

To summarize the present results, we found that two different fixed boundary conditions have an effect on the magnetic friction as an effective field; the anti-parallel and the parallel boundary conditions have disordering and ordering effects, respectively. In other words, the anti-parallel boundary conditions raise the effective temperature of the system and the parallel boundary conditions lower it. These effects emerge at the sliding boundary when the system behaves as a one-dimensional system, but vanish in the two-dimensional limit. The crossover between the one dimension and the two dimensions occurs below the size $L_z = 64$ in the limit $L_x \to \infty$.

The difference of the magnetic frictions under the two boundary conditions is maximized when the temperature of the system is near the boundary critical temperature and the system is sufficiently thin. Therefore we propose to manipulate the magnetic friction by switching the one boundary condition into the other of the system in the boundary criticality.

For future works, we are going to investigate the following:

- the divergence of derivatives of the *boundary* heat capacity in the limit of $L_z \to \infty$;
- the behavior of the correlation length itself;
- the dimensional crossover from the viewpoint of critical exponents.

We also intend to see whether dimensional crossovers occur in models with other spatial dimensions or continuous symmetries.

Appendix A

Analysis based on Stochastic Matrices

In this appendix, we prove the existence of the non-equilibrium stationary state in our model with sliding of arbitrary velocity. In the first section, we discuss the formulation in terms of stochastic matrices. In the following two sections, we prove based on Ref. [28] several facts for stochastic matrices, which ensures that almost all Monte Carlo simulations converge to a unique equilibrium state. In the last two sections, we propose a way to construct the matrix for both equilibrium cases and non-equilibrium stationary cases, and discuss the distributions of their eigenvalues in terms of the convergence.

A.1 A Simple Example: Stochastic Ising Model with N-spins

We now consider a matrix form of the stochastic process. For example, the one-dimensional Ising chain with N-spin has 2^N states. If we label each of the states by $i = 1, 2, \ldots, 2^N$, we can write the stochastic time evolution of the system by the existence probability $p_i(t)$ that the system is in the ith state at a time t and the transition probability T_{ij} such that the system in the jth state changes to the ith state.

We additionally define the conditional probability $\tilde{p}_{ij}(t)$ that the system in the jth state at a time t changes to the ith state at the next time $t+1$. Using the conditional probability, we can derive the relation between the existence probability $p_i(t)$ and the transition probability T_{ij} as

$$\tilde{p}_{ij}(t+1) = T_{ij} p_j(t) \quad \text{for } 1 \leq i, j \leq 2^N. \tag{A.1}$$

From a property of the probability, it should hold that $\sum_{i=1}^{2^N} p_i(t) = 1$ and $p_i(t) \geq 0$ ($i = 1, 2, \ldots, 2^N, t \in \mathbb{R}$). The conditional probability $\tilde{p}_{ij}(t)$ should also satisfy the condition that $\sum_{j=1}^{2^N} \tilde{p}_{ij}(t) = p_i(t+1)$ ($i = 1, 2, \ldots, 2^N, t \in \mathbb{R}$). Then we have

$$p_i(t+1) = \sum_{j=1}^{2^N} \tilde{p}_{ij}(t+1) = \sum_{j=1}^{2^N} T_{ij} p_j(t) \quad \text{for } 1 \leq i \leq 2^N,\ t \in \mathbb{R}. \tag{A.2}$$

In other words, the system can be described by the probability vector

$$\boldsymbol{p}(t) := {}^{\mathrm{t}}(p_1(t), p_2(t), \ldots, p_{2^N}(t)) \tag{A.3}$$

and the stochastic matrix $\hat{T} := (T_{ij})$ as

$$\boldsymbol{p}(t+1) = \hat{T}\boldsymbol{p}(t) \quad \text{for } t \in \mathbb{R}. \tag{A.4}$$

We have to consider such the matrix when we discuss the convergence to the stationary state or its uniqueness. These discussions are valid for general Ω-dimensional state spaces, and thus we denote the number of states by Ω from now on.

A.2 General Theory of Stochastic Matrices

In this section we discuss the conditions which ensure the convergence of a Monte Carlo simulation to a unique stationary state. We first define the stochastic matrix and discuss fundamental properties of the stochastic matrix. We next discuss a properties which result from an additional condition called *weak/strong connectivity*, and thereby show the existence and the uniqueness of a stationary state. We also see that we can construct a stochastic matrix which leads to any desired stationary state under the *detailed-balanced condition*.

From the condition $\sum_{i=1}^{\Omega} p_i(t) = 1$ and $p_i(t) \geq 0$ $(i = 1, 2, \ldots, \Omega, t \in \mathbb{R})$, we have a set of properties $\sum_{i=1}^{\Omega} T_{ij} = 1$, $T_{ij} \geq 0$ $(1 \leq i \leq \Omega)$. Any matrix with these conditions is called a *stochastic matrix* and shows the following interesting property:

Lemma A.2.1. Let $\hat{T}$ be a stochastic matrix. Then all absolute values of eigenvalue are less than or equal to unity. For any eigenvector $\boldsymbol{x} = {}^{\mathrm{t}}\{x_1, x_2, \ldots, x_\Omega\}$ which does *not* belong to the eigenvalue 1, it additionally holds that

$$\sum_{i=1}^{\Omega} x_j = 0. \tag{A.5}$$

We now define the vector $\boldsymbol{d} := {}^{\mathrm{t}}(1, 1, \ldots, 1)$ to prove all facts after this.

Proof. For any stochastic matrix $\hat{T}$, we have

$$\left({}^{\mathrm{t}}\hat{T}\boldsymbol{d}\right)_i = \sum_{j=1}^{\Omega} \left({}^{t}T\right)_{ij} d_j = \sum_{j=1}^{\Omega} T_{ji} d_j = \sum_{j=1}^{\Omega} T_{ji} = 1 \quad \text{for } i = 1, 2, \ldots, \Omega, \tag{A.6}$$

$$\iff \quad {}^{\mathrm{t}}\hat{T}\boldsymbol{d} = \boldsymbol{d}. \tag{A.7}$$

Therefore the matrix ${}^{\mathrm{t}}\hat{T}$ has at least an eigenvalue 1. The eigenequation for the matrix ${}^{\mathrm{t}}\hat{T}$ are rewritten as

$$\det\left[\lambda\hat{I}_\Omega - {}^{\mathrm{t}}\hat{T}\right] = \det\left[{}^{\mathrm{t}}\left(\lambda\hat{I}_\Omega - \hat{T}\right)\right] = \det\left[\lambda\hat{I}_\Omega - \hat{T}\right], \tag{A.8}$$

and then the set of eigenvalues of $\hat{T}$ is equal to that of ${}^{\mathrm{t}}\hat{T}$. Therefore the matrix $\hat{T}$ has at least an eigenvalue 1. A general eigenvalue equation of $\hat{T}$ can be written as

$$\hat{T}\boldsymbol{x}_n = \lambda_n \boldsymbol{x}_n, \tag{A.9}$$

where $\boldsymbol{x}_n = {}^{\mathrm{t}}(x_{n,1}, x_{n,2}, \ldots, x_{n,\Omega})$ is its eigenvector. We have

$$((\text{l.h.s of A.9}), \boldsymbol{d}) = (\hat{T}\boldsymbol{x}_\lambda, \boldsymbol{d}) = (\boldsymbol{x}_\lambda, {}^{\mathrm{t}}\hat{T}\boldsymbol{d}) = (\boldsymbol{x}_\lambda, \boldsymbol{d}), \tag{A.10}$$

$$((\text{r.h.s of A.9}), \boldsymbol{d}) = (\lambda\boldsymbol{x}_\lambda, \boldsymbol{d}) = \lambda(\boldsymbol{x}_\lambda, \boldsymbol{d}). \tag{A.11}$$

$$\iff (1-\lambda)(\boldsymbol{x}_\lambda, \boldsymbol{d}) = 0 \iff \lambda = 1 \text{ or } (\boldsymbol{x}_\lambda, \boldsymbol{d}) = 0. \tag{A.12}$$

$$\implies \sum_{i=1}^{\Omega} x_{\lambda,i} = 0 \quad \text{if } \lambda \neq 1. \tag{A.13}$$

We additionally define the vector $\boldsymbol{y}_\lambda := {}^{\mathrm{t}}(|x_{\lambda,1}|, |x_{\lambda,2}|, \ldots, |x_{\lambda,\Omega}|)$ for any λ. From the equation $\sum_{j=1}^{\Omega} T_{ij}x_{\lambda,j} = \lambda x_i (i = 1, 2, \ldots, \Omega)$, we have

$$\left|\sum_{j=1}^{\Omega} T_{ij}x_{\lambda,j}\right| \leq \sum_{j=1}^{\Omega} T_{ij}|x_{\lambda,j}| \quad (\because T_{ij} \geq 0 \quad \text{for } j = 1, 2, \ldots, \Omega) \tag{A.14}$$

$$= \left(\hat{T}\boldsymbol{y}_\lambda\right)_i \quad \text{for } i = 1, 2, \ldots, \Omega. \tag{A.15}$$

The left hand-side of (A.15) are rewritten as

$$\left|\sum_{j=1}^{\Omega} T_{ij}x_{\lambda,j}\right| = |\lambda x_{\lambda,j}| = |\lambda| \times |x_{\lambda,j}| = |\lambda| \times (\boldsymbol{y}_\lambda)_j, \tag{A.16}$$

and thus we have

$$|\lambda| \times (\boldsymbol{y}_\lambda)_j \leq \left(\hat{T}\boldsymbol{y}_\lambda\right)_i, \tag{A.17}$$

$$\iff |\lambda| \times (\boldsymbol{y}_\lambda, \boldsymbol{d}) \leq \left(\hat{T}\boldsymbol{y}_\lambda, \boldsymbol{d}\right) = \left(\boldsymbol{y}_\lambda, {}^{\mathrm{t}}\hat{T}\boldsymbol{d}\right) = (\boldsymbol{y}_\lambda, \boldsymbol{d}), \tag{A.18}$$

$$\iff |\lambda| \leq 1. \tag{A.19}$$

□

Definition A.2.1. For an arbitrary $1 \leq i, j \leq \Omega$, if there exists an $n(i,j) > 0$ such that

$$\left(\hat{T}^{n(i,j)}\right)_{ij} > 0, \tag{A.20}$$

the matrix $\hat{T}$ is called *weakly connected*. Note that for any $n' > n(i,j)$ it does *not* follow that $\left(\hat{T}^{n'}\right)_{ij} > 0$.

We limit the class of stochastic matrices to that of weakly connected ones from now on. To make the proofs of the theorems below easier, we also define the matrix $\hat{\mathcal{T}}_\epsilon$ ($\epsilon > 0$) and discuss its properties. Denoting the maximum value of $n(i,j)$ by $n_{\max} := \max_{1 \le i,j \le \Omega} [n(i,j)]$ and defining the matrix $\hat{\mathcal{T}}_\epsilon := \left(\hat{I}_\Omega + \epsilon \hat{T}\right)^{n_{\max}}$, we have

$$\left(\hat{\mathcal{T}}_\epsilon\right)_{ij} = \left(\left(\hat{I}_\Omega + \epsilon\hat{T}\right)^{n_{\max}}\right)_{ij} = \sum_{k=1}^{n_{\max}} \binom{n_{\max}}{k} \left(\hat{I}_\Omega^k \left(\epsilon\hat{T}\right)^{n_{\max}-k}\right)_{ij} \tag{A.21}$$

$$= \sum_{k=1}^{n_{\max}} \binom{n_{\max}}{k} \epsilon^{n_{\max}-k} \left(\hat{T}^{n_{\max}-k}\right)_{ij} \ge 0 \quad (\because T_{ij} > 0) \quad \text{for } 1 \le i,j \le \Omega. \tag{A.22}$$

For the eigenvector $\boldsymbol{x}_1 = {}^{\mathrm{t}}(x_{1,1}, x_{1,2}, \ldots, x_{1,\Omega})$, which belongs to the eigenvalue 1, it holds that

$$\hat{\mathcal{T}}_\epsilon \boldsymbol{x}_1 = \sum_{k=1}^{n_{\max}} \binom{k}{n_{\max}} \epsilon^{n_{\max}-k} \hat{T}^{n_{\max}} \boldsymbol{x}_1 \tag{A.23}$$

$$= \sum_{k=1}^{n_{\max}} \binom{k}{n_{\max}} \epsilon^{n_{\max}-k} \boldsymbol{x}_1 \tag{A.24}$$

$$= (1+\epsilon)^{n_{\max}} \boldsymbol{x}_1, \tag{A.25}$$

and each component is

$$\sum_{j=1}^{\Omega} \left(\hat{\mathcal{T}}_\epsilon\right)_{ij} x_{1,j} = (1+\epsilon)^{n_{\max}} x_{1,i} \quad \text{for } i = 1, 2, \ldots, \Omega. \tag{A.26}$$

Lemma A.2.2. We can decompose the vector into a phase factor and a positive vector as follows:

$$\boldsymbol{x}_1 = \mathrm{e}^{i\theta} \boldsymbol{u}_1, \tag{A.27}$$

where θ is the phase and $\boldsymbol{u}_1$ is the vector with all positive components.

Proof. If components of the vector $\boldsymbol{x}_1$ are *not* common such that $\sum_{i=1}^{\Omega} |x_{1,i}| > |\sum_{i=1}^{\Omega} x_{1,i}|$ holds, we have

$$\left| \sum_{j=1}^{\Omega} \left(\hat{\mathcal{T}}_\epsilon\right)_{ij} x_{1,j} \right| < \sum_{j=1}^{\Omega} \left(\hat{\mathcal{T}}_\epsilon\right)_{ij} |x_{1,j}| = (1+\epsilon)^{n_{\max}} |x_{1,i}|. \tag{A.28}$$

On the other hand, the row-wise sum of the matrix $\hat{\mathcal{T}}_\epsilon$ are

$$\sum_{i=1}^{\Omega} \left(\hat{\mathcal{T}}_\epsilon\right)_{ij} = \sum_{k=1}^{n_{\max}} \binom{k}{n_{\max}} \epsilon^{n_{\max}-k} \sum_{i=1}^{\Omega} \left(\hat{T}^{n_{\max}-k}\right)_{ij} = (1+\epsilon)^{n_{\max}}. \tag{A.29}$$

Then we have

$$\sum_{i=1}^{\Omega}\sum_{j=1}^{\Omega}\left(\hat{\mathcal{T}}_\epsilon\right)_{ij}|x_{1,j}| = (1+\epsilon)^{n_{\max}}\sum_{j=1}^{\Omega}|x_{1,j}| > (1+\epsilon)^{n_{\max}}\sum_{i=1}^{\Omega}|x_{1,i}|, \tag{A.30}$$

but it is the contradiction caused from our assumption $\sum_{i=1}^{\Omega}|x_{1,i}| > |\sum_{i=1}^{\Omega}x_{1,i}|$. Furthermore the left-hand side of (A.26) is positive because $n_{\max}$ is the maximum value of $n(i,j)$, and therefore the right-hand side is also positive $x_{1,i} > 0$ $(i = 1, 2, \ldots, \Omega)$. □

Lemma A.2.3. The eigenspace of the matrix $\hat{\mathcal{T}}_\epsilon$, which belongs to the eigenvalue 1, is *one-dimensional*.

Proof. If we have two different eigenvectors which belongs to the eigenvalue 1, we can write their eigenequations by two different *positive vectors* as

$$\hat{T}\boldsymbol{u}_1 = \boldsymbol{u}_1, \tag{A.31}$$

$$\hat{T}\boldsymbol{v}_1 = \boldsymbol{v}_1. \tag{A.32}$$

For their any linear superposition, we also have

$$\hat{T}(\boldsymbol{u}_1 + t\boldsymbol{v}_1) = \boldsymbol{u}_1 + t\boldsymbol{v}_1, \quad \text{for any } t \in \mathbb{R}. \tag{A.33}$$

If two eigenvectors $\boldsymbol{u}_1$ and $\boldsymbol{v}_1$ are not parallel to each other, we can make a non-trivial vector with a certain value of t such that $(\boldsymbol{u}_1 + t\boldsymbol{v}_1)_l = 0$ for an lth element. However it is the contradiction with the fact $x_{1,i} > 0$ $(i = 1, 2, \ldots, \Omega)$. Therefore we have no eigenspaces more than one which belongs to the eigenvalue 1. □

Definition A.2.2. If there exists a number $N_0 > 0$ such that

$$\left(\hat{T}^{N_0}\right)_{ij} > 0 \tag{A.34}$$

for an arbitrary $1 \le i, j \le \Omega$, the matrix $\hat{T}$ is called *strongly connected*.

We additionally limit the class of stochastic matrices to that of strongly connected ones from now on.

Theorem A.2.4. Unity is the only eigenvalue of absolute value 1.

Proof. We now have $\hat{T}^m\boldsymbol{u}_n = {\lambda_n}^m\boldsymbol{u}_n$, where $\boldsymbol{u}_n = {}^{\mathrm{t}}(u_{n,1}, u_{n,2}, \ldots, u_{n,\Omega})$ is the eigenvector which belongs to an eigenvalue λ. Their components are written as

$$\sum_{j=1}^{\Omega}\left(\hat{T}^n\right)_{ij}u_{\lambda,j} = \lambda^n\boldsymbol{u}_{\lambda,i} \quad \text{for } i = 1, 2, \ldots, \Omega. \tag{A.35}$$

We can divide conditions for λ into the following two cases:

Case 1: $\sum_{i=1}^{\Omega} |u_{\lambda,i}| > |\sum_{i=1}^{\Omega} u_{\lambda,i}|$**,**
We have

$$\sum_{j=1}^{\Omega} \left(\hat{T}^n\right)_{ij} |u_{\lambda,j}| > |\sum_{j=1}^{\Omega} \left(\hat{T}^n\right)_{ij} u_{\lambda,j}| = |\lambda^n| \times |u_{\lambda,i}|, \quad \text{for } i = 1, 2, \ldots, \Omega. \tag{A.36}$$

$$\iff \quad |\lambda^n| < 1 \quad \iff \quad |\lambda| < 1. \tag{A.37}$$

Case 2: $\sum_{i=1}^{\Omega} |u_{\lambda,i}| = |\sum_{i=1}^{\Omega} u_{\lambda,i}|$**.**
We have

$$\sum_{i=1}^{\Omega} \sum_{j=1}^{\Omega} \left(\hat{T}^n\right)_{ij} u_{\lambda,j} = \sum_{j=1}^{\Omega} u_{\lambda,j} = \lambda^n \sum_{i=1} u_{\lambda,i}. \tag{A.38}$$

$$\iff \quad \lambda^n = 1 \quad \left(\because \boldsymbol{u}_\lambda \neq \boldsymbol{0}, u_{\lambda,i} \geq 0 \Rightarrow \sum_{i=1}^{\Omega} u_{\lambda,i} > 0 \right). \tag{A.39}$$

Thus the eigenvalue 1 is the only eigenvalue of absolute value 1. □

Lemma A.2.5. The vector $\lim_{N\to\infty} \hat{T}^N \boldsymbol{r} = \boldsymbol{0}$ for any $\boldsymbol{r} \in \mathbb{C}$ is orthogonal to $\boldsymbol{d}$.

Proof. For an arbitrary vector $\boldsymbol{r}$, we can decompose it into its real and imaginary parts as $\boldsymbol{r} = \boldsymbol{r}_{\mathrm{R}} + i\boldsymbol{r}_{\mathrm{I}}$. Since the condition $(\boldsymbol{r}, \boldsymbol{d}) = 0$ is equivalent to $\sum_{i=1}^{\Omega} r_i = 0$, we have

$$\sum_{j \in I_+} r_j + \sum_{j \in I_-} r_j = 0, \tag{A.40}$$

where $I_\pm := \{j \mid r_j \gtrless 0, 1 \leq j \leq \Omega\}$. Note that $\sum_{j\in I_+} r_j = \sum_{j\in I_-} |r_j|$. Thus we have

$$\sum_{j \in I_+} r_j = \sum_{j \in I_-} |r_j| = \|\boldsymbol{r}\|_1/2. \tag{A.41}$$

Since $\hat{T}$ is strongly connected, there is an integer N_0 such that $\left(\hat{T}^{N_0}\right)_{ij} > 0$ for an arbitrary $1 \leq i, j \leq \Omega$. For N_0, we have

$$\left(\hat{T}^{N_0}\boldsymbol{r}\right) = \sum_{j=1}^{\Omega} \left(\hat{T}^{N_0}\right)_{ij} r_j = \sum_{j\in I_+} \left(\hat{T}^{N_0}\right)_{ij} r_j - \sum_{j\in I_-} \left(\hat{T}^{N_0}\right)_{ij} |r_j| \tag{A.42}$$

$$= \sum_{j=1}^{\Omega} \left(\hat{T}^{N_0}\right)_{ij} r_j - 2\sum_{j\in I_-} \left(\hat{T}^{N_0}\right)_{ij} |r_j| \tag{A.43}$$

$$\leq \sum_{j=1}^{\Omega} \left(\hat{T}^{N_0}\right)_{ij} r_j - 2\delta_{N_0} \sum_{j\in I_-} |r_j| \tag{A.44}$$

$$= \sum_{j=1}^{\Omega} \left(\hat{T}^{N_0}\right)_{ij} r_j - \delta_{N_0} \|\boldsymbol{r}\|_1, \tag{A.45}$$

where $\delta_{N_0} := \min_{1\leq i,j\leq\Omega}\left[\left(\hat{T}^{N_0}\right)_{ij}\right]$ for $i = 1, 2, \ldots, \Omega$. Note that there exists $\delta_{N_0} > 0$ for the strongly connected matrix $\hat{T}$. Similarly we have

$$\left(\hat{T}^{N_0}\boldsymbol{r}\right) = \sum_{j=1}^{\Omega}\left(\hat{T}^{N_0}\right)_{ij} r_j = \sum_{j\in I_+}\left(\hat{T}^{N_0}\right)_{ij} r_j - \sum_{j\in I_-}\left(\hat{T}^{N_0}\right)_{ij}|r_j| \tag{A.46}$$

$$=2\sum_{j\in I_+}\left(\hat{T}^{N_0}\right)_{ij} r_j - \sum_{j=1}^{\Omega}\left(\hat{T}^{N_0}\right)_{ij}|r_j| \tag{A.47}$$

$$\geq 2\delta_{N_0}\sum_{j\in I_+} r_j - \sum_{j=1}^{\Omega}\left(\hat{T}^{N_0}\right)_{ij}|r_j| \tag{A.48}$$

$$=\delta_{N_0}\|\boldsymbol{r}\|_1 - \sum_{j=1}^{\Omega}\left(\hat{T}^{N_0}\right)_{ij}|r_j| \quad \text{for } i = 1, 2, \ldots, \Omega. \tag{A.49}$$

Combining them, we have

$$|\left(\hat{T}^{N_0}\boldsymbol{r}\right)| \leq \sum_{j=1}^{\Omega}\left(\hat{T}^{N_0}\right)_{ij}|r_j| - \delta_{N_0}\|\boldsymbol{r}\|_1 \quad \text{for } i = 1, 2, \ldots, \Omega, \tag{A.50}$$

and then it holds that

$$\|\hat{T}^{N_0}\boldsymbol{r}\|_1 = \sum_{i=1}^{\Omega}|\left(\hat{T}^{N_0}\boldsymbol{r}\right)_i| \leq \sum_{j=1}^{\Omega}|r_j| - N_0\delta_{N_0}\|\boldsymbol{r}\|_1 = (1 - N\delta_{N_0})\|\boldsymbol{r}\|_1. \tag{A.51}$$

The vector $\hat{T}^{N_0}\boldsymbol{r}$ is also orthogonal to the vector $\boldsymbol{d}$:

$$\left(\hat{T}^{N_0}\boldsymbol{r}, \boldsymbol{d}\right) = \left(\boldsymbol{r}, {}^{\mathrm{t}}\left(\hat{T}^{N_0}\right)\boldsymbol{d}\right) = \left(\boldsymbol{r}, \left({}^{\mathrm{t}}\hat{T}\right)^{N_0}\boldsymbol{d}\right) = (\boldsymbol{r}, \boldsymbol{d}) = 0. \tag{A.52}$$

Then, for any positive integer l, we can repeat this discussion as

$$\|\hat{T}^{N_0 l}\boldsymbol{r}\|_1 \leq (1 - N_0\delta_{N_0})^l\|\boldsymbol{r}\|_1. \tag{A.53}$$

Since $N_0 > 0, \delta_{N_0} > 0$ and thus $1 - N_0\delta_{N_0} < 0$, we have

$$\lim_{l\to\infty}(1 - N_0\delta_{N_0})^l\|\boldsymbol{r}\|_1 = 0. \tag{A.54}$$

$$\iff \quad \lim_{l\to\infty}\|\hat{T}^{N_0 l}\boldsymbol{r}\|_1 = 0. \tag{A.55}$$

Thus, for an arbitrary positive integer N, we have

$$\lim_{N\to\infty}\|\hat{T}^{N}\boldsymbol{r}\|_1 = 0. \tag{A.56}$$

□

Lemma A.2.6. We can write any vector $\boldsymbol{x}$ as the superposition of $\boldsymbol{u}_1$ and $\boldsymbol{r}$.

Proof. Defining the coefficient $c_{1,\boldsymbol{x}} := (\boldsymbol{x}, \boldsymbol{d})/(\boldsymbol{u}_1, \boldsymbol{d})$ and the vector $\boldsymbol{r}_{\boldsymbol{x}} := \boldsymbol{x} - c_{1,\boldsymbol{x}}\boldsymbol{u}_1$, we have

$$(\boldsymbol{r}_{\boldsymbol{x}}, \boldsymbol{d}) = (\boldsymbol{x}, \boldsymbol{d}) - \frac{(\boldsymbol{x}, \boldsymbol{d})}{(\boldsymbol{u}_1, \boldsymbol{d})}(\boldsymbol{u}_1, \boldsymbol{d}) = 0, \tag{A.57}$$

$$\boldsymbol{x} = c_{1,\boldsymbol{x}}(\boldsymbol{u}_1, \boldsymbol{d}) + \boldsymbol{r}_{\boldsymbol{x}}. \tag{A.58}$$

□

Theorem A.2.7. The limit $\lim_{N\to\infty} \hat{T}^N \boldsymbol{p}^{(0)}$ is independent of the initial vector $\boldsymbol{p}^{(0)}$:

$$\lim_{N\to\infty} \hat{T}^N \boldsymbol{p}^{(0)} = \frac{\boldsymbol{u}_1}{\|\boldsymbol{u}_1\|_1}, \tag{A.59}$$

where the vector $\boldsymbol{p}^{(0)} = {}^{\mathrm{t}}\left\{p_1^{(0)}, p_2^{(0)}, \ldots, p_\Omega^{(0)}\right\}$ is in the class of probability vectors normalized as $\sum_{i=1}^{\Omega} p_i^{(0)} = 1$.

Proof. From the theorem A.2.6, we have

$$\hat{T}^N \boldsymbol{p}^{(0)} = c_{1,\boldsymbol{p}^{(0)}} \hat{T}^N \boldsymbol{u}_1 + \hat{T}^N \boldsymbol{r}_{\boldsymbol{p}^{(0)}} = c_{1,\boldsymbol{p}^{(0)}} \boldsymbol{u}_1 + \hat{T}^N \boldsymbol{r}_{\boldsymbol{p}^{(0)}}. \tag{A.60}$$

Its limit $N \to \infty$ is taken as

$$\lim_{N\to\infty} \hat{T}^N \boldsymbol{p}^{(0)} = c_{1,\boldsymbol{p}^{(0)}} \boldsymbol{u}_1 + \lim_{N\to\infty} \hat{T}^N \boldsymbol{r}_{\boldsymbol{p}^{(0)}} = c_{1,\boldsymbol{p}^{(0)}} \boldsymbol{u}_1. \tag{A.61}$$

Using the matrix $\hat{A} := \boldsymbol{u}_1{}^{\mathrm{t}}\boldsymbol{d}/(\boldsymbol{u}_1, \boldsymbol{d})$, we have

$$\left(\hat{A}\boldsymbol{p}^{(0)}\right)_i = \sum_{j=1}^{\Omega} \frac{(\boldsymbol{u}_1)_i}{(\boldsymbol{u}_1, \boldsymbol{d})} \left(\boldsymbol{p}^{(0)}\right)_j = \left(\boldsymbol{p}^{(0)}, \boldsymbol{d}\right) \frac{(\boldsymbol{u}_1)_i}{(\boldsymbol{u}_1, \boldsymbol{d})}, \quad \text{for } i = 1, 2, \ldots, \Omega. \tag{A.62}$$

It leads to

$$\hat{A}\boldsymbol{p}^{(0)} = \frac{(\boldsymbol{u}_1)_i}{(\boldsymbol{u}_1, \boldsymbol{d})} \boldsymbol{p}^{(0)} = c_{1,\boldsymbol{p}^{(0)}} \boldsymbol{p}^{(0)}. \tag{A.63}$$

The limit $N \to \infty$ for $\hat{T}^N \boldsymbol{p}^{(0)}$ is rewritten by a simple multiplication as follows:

$$\lim_{N\to\infty} \hat{T}^N \boldsymbol{p}^{(0)} = \frac{\boldsymbol{u}_1{}^{\mathrm{t}}\boldsymbol{d}}{(\boldsymbol{u}_1, \boldsymbol{d})} \boldsymbol{p}^{(0)}. \tag{A.64}$$

The expression (A.64) lead to the relation $\lim_{N\to\infty} \hat{T}^N \boldsymbol{p}^{(0)} = \boldsymbol{u}_1/\|\boldsymbol{u}_1\|_1$. Indeed it holds that

$$\frac{\boldsymbol{u}_1{}^{\mathrm{t}}\boldsymbol{d}}{(\boldsymbol{u}_1, \boldsymbol{d})} \left(\boldsymbol{p}^{(0)}\right)_i = \frac{\sum_{j=1}^{\Omega} (\boldsymbol{u}_1)_i (\boldsymbol{d})_j \left(\boldsymbol{p}^{(0)}\right)_j}{(\boldsymbol{u}_1, \boldsymbol{d})} = \frac{u_{1,i}}{\|\boldsymbol{u}_1\|_1}, \tag{A.65}$$

and thus we have

$$\lim_{N\to\infty} \hat{T}^N \boldsymbol{p}^{(0)} = \frac{\boldsymbol{u}_1}{\|\boldsymbol{u}_1\|_1}. \tag{A.66}$$

□

Once we get a strongly connected stochastic matrix $\hat{T}$, its stationary distribution $\boldsymbol{u}_1/\|\boldsymbol{u}_1\|_1$ is determined independently of the initial distribution.

A.3 Construction of the Stochastic Matrix based on the Detailed Balanced Condition

On the other hand, we can also construct the inverse discussion. This means the *construction* of the matrix $\hat{T}'$ with a *desired* stationary distribution $\boldsymbol{p}'$. We can formulate such a procedure using the *detailed-balanced condition* as follows.

Definition A.3.1. The matrix $\hat{T}'$ satisfies the detailed-balanced condition if it holds that

$$T'_{ij}p'_j = T'_{ji}p'_i \quad \text{for } 1 \leq i, j \leq \Omega \tag{A.67}$$

for the stationary distribution $\boldsymbol{p}' = {}^{\mathrm{t}}(p'_1, p'_2, \ldots, p'_\Omega)$.

This property is simplified by summing over the subscription i as follows

$$\sum_{i=1}^{\Omega} T'_{ij}p'_j = p'_j = \sum_{i=1}^{\Omega} T'_{ji}p'_i = \left(\hat{T}\boldsymbol{p}'\right)_j, \quad \text{for } j = 1, 2, \ldots, \Omega. \tag{A.68}$$

Then if the detailed-balanced condition holds for a matrix $\hat{T}'$, the corresponding vector $\boldsymbol{p}'$ is the fixed point of the matrix $\hat{T}'$. Thus in order to obtain the matrix $\hat{T}'$ which leads any distribution $\boldsymbol{p}^{(0)}$ to the desired distribution $\boldsymbol{p}'$, we only have to construct each element T'_{ij} of the matrix according to the condition (A.67) and make the matrix strongly connected.

In Monte Carlo simulations of statistical mechanics, we calculate the equilibrium distribution $\boldsymbol{p}_{\mathrm{eq}}(\beta)$ at an inverse temperature β using an initial state i_0 and a rule of the stochastic process $i \to j \to j' \to \ldots$. We can regard the matrix construction method as a set of the stochastic process $i_0 \to j \to j' \to \ldots$ over all possible states $i_0 = 1, 2, \ldots, \Omega$.

The condition (A.67) or

$$\frac{T_{ij}}{T_{ji}} = \frac{p_i}{p_j} \tag{A.69}$$

is not sufficient to determine a concrete form of the matrix $\hat{T}$ and thus in general there is a degree of freedom in the form of $\hat{T}$. For Monte Carlo simulations of equilibrium statistical mechanics, this freedom also remains as follows:

$$\frac{T_{ij}(\beta)}{T_{ji}(\beta)} = \frac{p_i(\beta)}{p_j(\beta)} = \mathrm{e}^{-\beta(E_i - E_j)} \quad \text{for } 1 \leq i, j \leq \Omega, \tag{A.70}$$

where $T_{ij}(\beta)$ and $p_i(\beta)$ are the matrix corresponding to a simulation and the probability that the ith state emerges, respectively, at a fixed inverse temperature β. Nonetheless the relation (A.70) is important in that the rate of transition probabilities is always given by the difference of energies $\{E_1, E_2, \ldots, E_\Omega\}$, and thus we do *not* have to calculate the exact values of $\tilde{p}_i(\beta) := \exp\left[-\beta E_i\right] / Z(\beta)$, where $Z(\beta) := \sum_i \exp\left[-\beta E_i\right]$.

If we use the Metropolis algorithm for the N-spin system, each element of the matrix $T_{ij}(\beta)$ is written as follows.

$$T_{ij}(\beta) = \begin{cases} \frac{1}{N} \min\left[1, \mathrm{e}^{-\beta(E_i - E_j)}\right] & \text{for states } i, j \text{ mutually reacheable by a single flip,} \\ 0 & \text{for states } i, j \textit{ not} \text{ mutually reacheable by a single flip.} \end{cases} \tag{A.71}$$

The factor $1/N$ describes the random selection of a spin to flip.

We call the matrix with the condition (A.71) the *Metropolis matrix* and denote it by M_{ij} from now on.

Metropolis matrices generally have few non-zero elements because of not taking transitions between all energy eigenstates into account. Thus the Monte Carlo simulation with the Metropolis rate is very simple, but the convergence is not trivial. In the following subsections, we show the convergence for quite limited cases using the strong connectivity of the stochastic matrix.

A.3.1 Metropolis Matrix for the Model of the Size 3×2

We construct the Metropolis matrix $\hat{M}(\beta)$ for the model of size $L_x = 3$, $L_z = 2$ in a concrete form and verify that all elements of the sixth power of the matrix are non-zero. By the fact, we can see the existence of its unique stationary state in the long-time limit . In addition we investigate the distribution of the eigenvalues of $\hat{M}(\beta)$ for several temperatures and verify that the matrix $\hat{M}(\beta)$ has only one eigenvalue of unity and all other eigenvalues are inside the unit circle on the complex plane except for the case $\beta = 0$; see Fig. A.2.

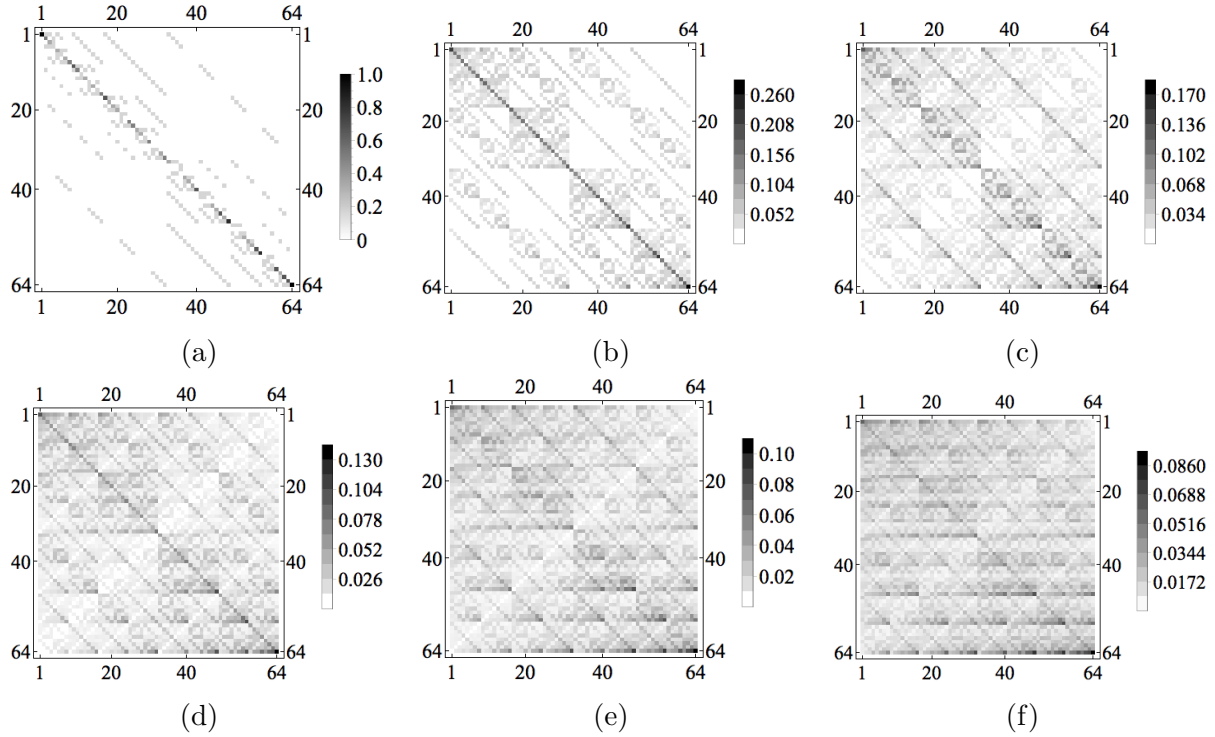

Figure A.1: The array plots of powers of $\hat{M}(\beta)$ of size $L_x = 3, L_z = 2$ and at the temperature $T = 10$: (a) $\hat{M}(\beta)$; (b) $\left(\hat{M}(\beta)\right)^2$; (c) $\left(\hat{M}(\beta)\right)^3$; (d) $\left(\hat{M}(\beta)\right)^4$; (e) $\left(\hat{M}(\beta)\right)^5$; (f) $\left(\hat{M}(\beta)\right)^6$.

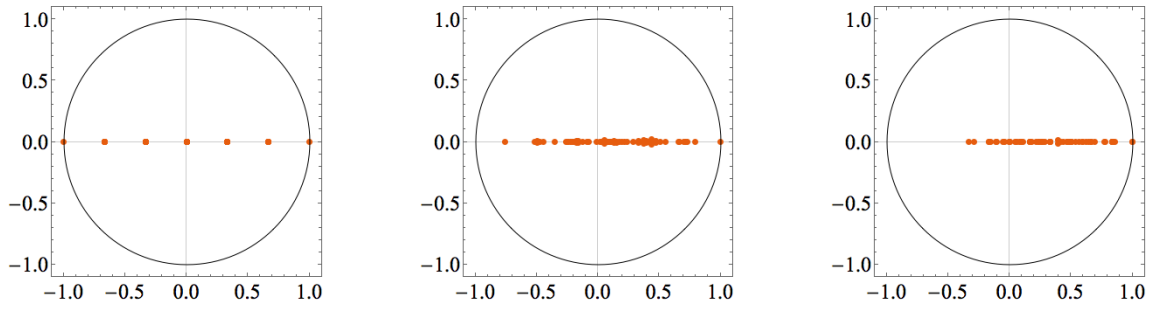

Figure A.2: The distributions of eigenvalues for $\hat{M}(\beta)$: (a) $\beta \to +0$; (b) $\beta = 0.1$; (c) $\beta \to +\infty$.

Bibliography

[1] A. Hucht, Phys. Rev. E **80**, 061138 (2009).

[2] M. Weiss and F.-J. Elmer, Phys. Rev. B **53**, 7539 (1996).

[3] M. Weiss and F.-J. Elmer, Zeitschrift für Phys. B Condens. Matter **104**, 55 (1997).

[4] I. García-Mata, O. V. Zhirov, and D. L. Shepelyansky, Eur. Phys. J. D **41**, 325 (2007).

[5] E. Meyer, Science **348**, 1089 (2015).

[6] A. Bylinskii, D. Gangloff, I. Counts, and V. Vuletić, Nat. Mater. **15**, 717 (2016).

[7] T. Novotný and B. Velický, Phys. Rev. Lett. **83**, 4112 (1999).

[8] N. Hosomi, A. Tanabe, M. Suzuki, and M. Hieda, Phys. Rev. B **75**, 064513 (2007).

[9] N. Hosomi and M. Suzuki, Phys. Rev. B **77**, 024501 (2008).

[10] N. Hosomi, J. Taniguchi, M. Suzuki, and T. Minoguchi, Phys. Rev. B **79**, 172503 (2009).

[11] M. Ternes, C. P. Lutz, C. F. Hirjibehedin, F. J. Giessibl, and A. J. Heinrich, Science **319**, 1066 (2008).

[12] M. Urbakh and E. Meyer, Nat. Mater. **9**, 8 (2010).

[13] S. H. Kim, D. B. Asay, and M. T. Dugger, Nano Today **2**, 22 (2007).

[14] D. S. Grierson and R. W. Carpick, Nano Today **2**, 12 (2007).

[15] N. Manini, G. Mistura, G. Paolicelli, E. Tosatti, and A. Vanossi, Adv. Phys. X **2**, 569 (2017).

[16] D. Kadau, A. Hucht, and D. E. Wolf, Phys. Rev. Lett. **101**, 137205 (2008).

[17] M. P. Magiera, S. Angst, A. Hucht, and D. E. Wolf, Phys. Rev. B **84**, 212301 (2011).

[18] B. Wolter, Y. Yoshida, A. Kubetzka, S.-W. Hla, K. von Bergmann, and R. Wiesendanger, Phys. Rev. Lett. **109**, 116102 (2012).

[19] T. Strunz and F.-J. Elmer, Phys. Rev. E **58**, 1601 (1998).

[20] T. Strunz and F.-J. Elmer, Phys. Rev. E **58**, 1612 (1998).

[21] Q. Meng, L. Wu, D. O. Welch, and Y. Zhu, Phys. Rev. B **91**, 224305 (2015).

[22] Q. Meng, L. Wu, D. O. Welch, and Y. Zhu, Phys. Rev. B **91**, 224306 (2015).

[23] A. Dayo, W. Alnasrallah, and J. Krim, Phys. Rev. Lett. **80**, 1690 (1998).

[24] C. Fusco, D. E. Wolf, and U. Nowak, Phys. Rev. B **77**, 174426 (2008).

[25] M. P. Magiera, L. Brendel, D. E. Wolf, and U. Nowak, Europhys. Lett. **87**, 26002 (2009).

[26] M. P. Magiera, L. Brendel, D. E. Wolf, and U. Nowak, Europhys. Lett. **95**, 17010 (2011).

[27] R. J. Glauber, J. Math. Phys. **4**, 294 (1963).

[28] T. Hara, *Lecture Note for Mathematics (in Japanese)* (http://www2.math.kyushu-u.ac.jp/~hara/lectures/11/tokuronA3-ho.pdf, 2011), pp. 1–42.